Experimental Investigations of Air Entrainment in Transition and Skimming Flows down a Stepped Chute

Application to Embankment Overflow Stepped Spillways

H. CHANSON (*Reader*) and L. TOOMBES (*Associate Lecturer*)

Dept of Civil Engineering, The University of Queensland, Brisbane QLD 4072, Australia

Fax : (61 7) 33 65 45 99

URL: http://www.uq.edu.au/~e2hchans

Email: h.chanson@mailbox.uq.edu.au

RESEARCH REPORT No. CE 158

Department of Civil Engineering

The University of Queensland

July, 2001

ISBN 1 864995297

ABSTRACT: Stepped spillways have been used for about 3,500 years. The last few decades have seen the development of new construction materials, design techniques and applications : e.g., embankment overtopping protection systems. Although it is commonly acknowledged that free-surface aeration is significant in stepped chutes, experimental data are scarce, often limited to very steep slopes ($\alpha \sim 50^o$). The paper presents an experimental study conducted in a large-size stepped chute ($\alpha = 22^o$, h = 0.1 m, W = 1 m). Observations demonstrate the existence of a transition flow pattern for intermediate flow rates between nappe and skimming flows. Detailed air-water flow measurements were conducted in both transition and skimming flows, immediately downstream of the inception point of free-surface aeration where uniform equilibrium flow conditions were not achieved. In skimming flows, a complete characterisation is developed for the distributions of void fraction, bubble count rate and velocity, and flow resistance is estimated including drag reduction effects. Transition flows exhibit significantly different air-water flow properties. They are highly aerated, requiring the design of comparatively high chute sidewalls. The design of embankment overflow stepped spillway is discussed in the light of the new results and design recommendations are provided. Major design issues include the step stability at the plunge point for high tailwater levels, the interactions between free-surface and seepage flows which could lead to further drag reduction, and secondary currents at the connection between steps and abutments.

Keywords : stepped spillway, air entrainment, two-phase flow properties, drag reduction, embankment overflow protection.

Table of contents

Notation

a	air-water specific area (1/m);
a_{mean}	depth-averaged air-water specific area (1/m);
C	air concentration defined as the volume of air per unit volume, also called void fraction;
C_{mean}	depth averaged air concentration defined as : $(1 - Y_{90}) * C_{mean} = d$;
C_p	inflow pressure coefficient defined as : $C_p = \frac{1}{\frac{1}{2} * \rho * g * d^2} * \int_0^d P(y) * dy$
D_H	hydraulic diameter (m); $D_H = 4*d*W/(W + 2*d)$ for a rectangular channel;
D_t	turbulent diffusivity (m^2/s) of air bubble in air-water flows;
D_o	dimensionless coefficient;
D'	dimensionless air bubble diffusivity (defined by CHANSON 1995b);
d	1- flow depth measured normal to the channel slope at the edge of a step; 2- characteristic depth (m) defined as : $d = \int_0^{Y_{90}} (1 - C) *dy$; 3- channel height (m);
d_c	critical flow depth (m); for a rectangular channel : $d_c = \sqrt[3]{q_w^2/g}$;
d_o	inflow depth (m);
F_{ab}	bubble count rate (Hz) : i.e., number of bubbles detected by the probe sensor per second;
$(F_{ab})_{max}$	maximum bubble count rate (Hz);
F_{ej}	average cavity ejection frequency (Hz);
f	Darcy friction factor for water flows;
f_d	equivalent Darcy friction factor estimate of the form drag;
f_e	Darcy friction factor of air-water flows
f_i	Darcy friction factor, neglecting air entrainment;
g	gravity constant (m/s^2) or acceleration of gravity; g = 9.80 m/s^2 in Brisbane;
H	total head (m);
h	height of steps (m) (measured vertically);
k	Von Karman constant;

K	inverse of the spreading rate of a turbulent shear layer;
K'	integration constant;
K^*	$K^* = \tanh^{-1}(\sqrt{0.1}) = 0.32745015...$;
k_s	cavity depth (m) (or roughness height);
L_{cav}	cavity length (m), or step cavity length (m) measured between step edges;
l	horizontal length of steps (m) (measured perpendicular to the vertical direction);
N	exponent of the velocity power law;
n	exponent;
P	pressure (Pa);
Q	discharge (m^3/s);
q	discharge per unit width (m^2/s);
R	normalised cross-correlation coefficient;
S_f	friction slope;
s	curvi-linear coordinate (m) measured in the flow direction
T	bubble travel time (s) for which the cross-correlation function is maximum;
Tu	turbulence intensity defined as : $Tu = u'/V$;
Tu'	characteristic turbulence intensity in air-water flows (App. IV);
t, t'	time (s);
U_W	clear-water flow velocity (m/s) : $U_W = q_W/d$;
u'	root mean square of longitudinal component of turbulent velocity (m/s);
u_r	bubble rise velocity (m/s);
$(u_r)_{Hyd}$	bubble rise velocity (m/s) in a hydrostatic pressure gradient;
V	velocity (m/s);
V_c	critical velocity (m/s); for a rectangular channel : $V_c = \sqrt[3]{g * q_w}$;
V_{90}	characteristic velocity (m/s) where the air concentration is 90%;
V_o	free-stream velocity (m/s);
W	channel width (m);
x	longitudinal distance (m);
Y_{90}	characteristic depth (m) where the air concentration is 90%;

y	1- distance (m) from the bottom measured perpendicular to the spillway invert; 2- distance (m) from the pseudo-bottom (formed by the step edges) measured perpendicular to the flow direction;

Greek symbols

α	channel slope;
Δx	distance between probe sensors (m);
δx	characteristic sensor size (m) in the flow direction;
δ_{BL}	boundary layer thickness (m);
δ_*	displacement thickness (m);
δ_M	momentum thickness (m);
λ	dimensionless coefficient;
μ	dynamic viscosity (N.s/m^2);
ν	kinematic viscosity (m^2/s);
π	π = 3.14159265358979323846264 3...;
ρ	density (kg/m^3);
σ	surface tension between air and water (N/m);
τ_o	boundary shear stress (Pa);
$\varnothing$	diameter (m);

Subscript

air	air flow;
c	critical flow conditions;
w	water flow;

Abbreviations

RCC	roller compacted concrete.

About the writers

Hubert Chanson received a degree of 'Ingénieur Hydraulicien' from the Ecole Nationale Supérieure d'Hydraulique et de Mécanique de Grenoble (France) in 1983 and a degree

Atomique' from the 'Institut National des Sciences et Techniques Nucléaires' in 1984. He worked for the industry in France as a R&D engineer at the Atomic Energy Commission from 1984 to 1986, and as a computer professional in fluid mechanics for Thomson-CSF between 1989 and 1990. From 1986 to 1988, he studied at the University of Canterbury (New Zealand) as part of a Ph.D. project. He was awarded a Doctor of Engineering from the University of Queensland in 1999 for outstanding research achievements in gas-liquid bubbly flows.

Hubert Chanson is a reader in environmental fluid mechanics and water engineering at the University of Queensland since 1990. His research interests include design of hydraulic structures, experimental investigations of two-phase flows, coastal hydrodynamics, water quality modelling, environmental management and natural resources. He is the author of four books : "Hydraulic Design of Stepped Cascades, Channels, Weirs and Spillways" (*Pergamon*, 1995), "Air Bubble Entrainment in Free-Surface Turbulent Shear Flows" (*Academic Press*, 1997), "The Hydraulics of Open Channel Flows : An Introduction" (*Butterworth-Heinemann*, 1999) and "The Hydraulics of Stepped Chutes and Spillways" (*Balkema*, 2001). His publication record includes over 180 international refereed papers and his work was cited over 600 times since 1990. Hubert Chanson has been active also as consultant for both governmental agencies and private organisations. He has been awarded five fellowships from the Australian Academy of Science. In 1995 he was a Visiting Associate Professor at National Cheng Kung University (Taiwan R.O.C.) and he was Visiting Research Fellow at Toyohashi University of Technology (Japan) in 1999 and 2001.

Hubert Chanson was the keynote lecturer at the 1998 ASME Fluids Engineering Symposium on Flow Aeration (Washington DC), at the Workshop on Flow Characteristics around Hydraulic Structures (Nihon University, Japan 1998) and at the first International Conference of the International Federation for Environmental Management System IFEMS'01 (Tsurugi, Japan 2001). He gave an invited lecture at the International Workshop on Hydraulics of Stepped Spillways (ETH-Zürich, 2000). He lectured several short courses in Australia and overseas (e.g. Taiwan).

Luke Toombes graduated a Bachelor in Civil Engineering (BEng., 1st Hon.) at the University of Queensland in 1994. He worked for the industry in Australia from 1995 to 1996 as a consulting engineer for Cullen, Grummitt & Roe Pty Ltd, with expertise in the design and management of ports and harbours, both in Australia and overseas. Between 1996 and 2001, he studied at the University of Queensland as part of a Ph.D. project investigating the air-water flow properties of stepped cascades.

Luke Toombes is an Associate Lecturer in fluid mechanics at the Department of Civil Engineering, the University of Queensland. His research interests include coastal processes, hydraulic engineering and hydraulic structures. His publication record includes 10 international refereed papers and two refereed research reports. His work was cited more than 10 times since 1997.

Part I - Experimental investigations in a 1V:2.5H stepped spillway model

1. Introduction

Stepped spillways have been used for about 3,500 years (CHANSON 2000,2001). During the 19th century, the design technique was common in Europe, North-America and Australia (e.g. SCHUYLER 1909, WEGMANN 1911, KELEN 1933, CHANSON 1997a) (Fig. 1-1A). By the end of the 19th century, it was understood that stepped chutes contributed significantly to the dissipation of the flow energy : e.g., the design of the Gold Creek and New Croton dam spillways (WEGMANN 1907, CHANSON and WHITMORE 1998). The interest in stepped cascades dropped however during the first half of the 20th century with new progresses in the energy dissipation characteristics of hydraulic jumps favouring the design of hydraulic jump stilling basins. Stilling basins allowed larger energy dissipation and smaller structures, leading to cheaper construction costs.

Fig. 1-1 - Photographs of stepped spillways
(A) Pas du Riot dam, Planfroy, France in June 1998 - Completed in 1873 (H = 36 m), design discharge : 65 m^3/s, 7 steps (h ~ 2.5 à 3 m), trapezoidal cross-section (base width ~ 3 m)

Since the 1970s, the regain of interest for the stepped spillway design has been associated with the development of new construction materials (e.g. roller compacted concrete RCC, polymer coated gabions), the introduction of new design techniques (e.g. overflow embankment dam protection systems with RCC and precast concrete blocks), and the development of new applications (e.g. re-oxygenation cascades) (Fig. 1-1B). Research on stepped chute hydraulics has been very active : i.e., one book, sixteen journal papers and twenty-six discussions listed in Global Books in Print™ and Science Citation Index™ for the period 1985-2000. However most studies prior to 1992 neglected the effects of free-surface aeration ('white waters'), until the first data by RUFF and FRIZELL (1994) and the analysis of CHANSON (1993a). Today experimental data on air entrainment down stepped chute are scarce, often limited to very steep slopes ($\alpha \sim 50^o$) as used for gravity dams (Table 1-1).

Table 1-1 - Detailed experimental investigations of air entrainment in stepped chutes

Reference	α deg.	q_W m^2/s	h m	Flow regime	Remarks
(1)	(2)	(3)	(4)	(5)	(6)
CHANSON and TOOMBES (1997, 2000)	3.4	0.038 to 0.163	0.143	Nappe flow	W = 0.5 m. Supercritical inflow (0.03-m nozzle thickness).
TOZZI et al. (1998)	52.2	0.23	0.053	Skimming flow	Inflow: uncontrolled smooth WES ogee crest followed by smaller first steps.
CHAMANI and RAJARATNAM (1999)	51.3 & 59	0.07 to 0.2	0.313 to 0.125	Skimming flow	W = 0.30 m. Inflow: un-controlled smooth WES ogee crest.
MATOS (2000)	53.1	0.08 to 0.2	0.08	Skimming flow	W = 1 m. Inflow: uncontrolled WES ogee crest, with small first steps built in the ogee development.
TOOMBES and CHANSON (2000)	3.4	0.08 to 0.136	0.143	Nappe flow	W = 0.25 m. Supercritical inflow (nozzle thickness : 0.028 to 0.040 m). Ventilated steps.
BOES (2000)	30 & 50	--	0.023 to 0.09	Skimming flow	W = 0.5 m. Inflow: pressurised intake.
OHTSU et al. (2000)	55	0.016 to 0.03	0.025	Skimming flow	W = 0.3 m. Inflow: uncontrolled broad-crest.
Present study	21.8	0.04 to 0.18	0.1	Transition & Skimming flows	W = 1 m. Inflow: uncontrolled broad-crest.

Fig. 1-1 - Photographs of stepped spillways
(B) Riou dam, France in November 1994 - Completed in 1990 (H = 22 m), design discharge : 1.5 m^2/s, width : 96 m, h = 0.43 m, RCC construction

It is the purpose of this study to provide a comprehensive database on air-water flows down stepped chutes. Measurements were conducted on a large facility (h = 0.1 m, W = 1 m) with a precise instrumentation. (Based upon a Froude similitude, the large size of the facility ensures that the experimental results may be extrapolated to prototype with negligible scale effects for geometric scaling ratios less than 10:1.) Two flow regimes were investigated, providing a broad spectrum of flow conditions. A complete characterisation of the air-water flow properties is provided. The results are discussed in the context of embankment overflow stepped spillways and design recommendations are provided.

2. Experimental apparatus and instrumentation

Experiments were conducted at the University of Queensland in a 2.7-m long, 1-m wide, 21.8º slope chute (Table 2-1). Waters were supplied from a large feeding basin (1.5-m deep, surface area 6.8 m × 4.8 m) leading to a sidewall convergent with a 4.8:1 contraction ratio. The test section consisted of a broad-crested weir (1-m wide, 0.6-m long, with upstream rounded corner (0.057-m radius)) followed by nine identical steps (h = 0.1 m, l = 0.25 m) made of marine ply. The stepped chute was 1-m wide with

perspex sidewalls, followed by a horizontal concrete-invert canal ending in a dissipation pit.

Fig. 2-1 - Definition sketch of the test section

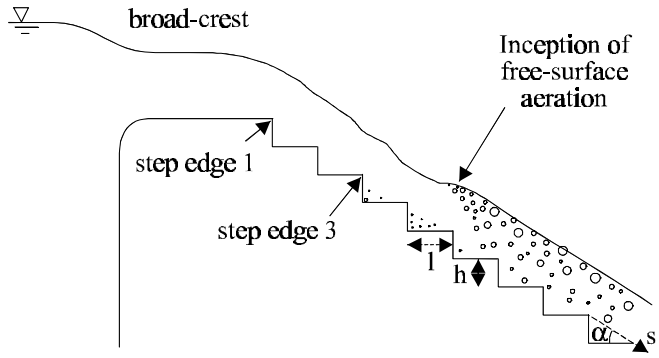

Table 2-1 - Summary of experimental flow conditions

Ref.	Q_w m^3/s	Location of inception of free-surface aeration	Flow regime	Remarks
(1)	(2)	(3)	(4)	(5)
Series 1				Single-tip probe
	0.182	Step edge 6	Skimming flow	Run Q5
	0.164	Step edge 6	Skimming flow	Run Q6
	0.147	Step edge 5	Skimming flow	Run Q7
	0.130	Step edge 5	Skimming flow	Run Q8
	0.124	Step edge 5	Skimming flow	Run Q1
	0.114	Step edge 5	Skimming flow	Run Q9
	0.103	Step edge 4	Skimming flow	Run Q2
	0.099	Step edge 4	Transition flow	Run Q10
	0.085	Step edge 4	Transition flow	Run Q11
	0.080	Step edge 4	Transition flow	Run Q3
	0.071	Step edge 3	Transition flow	Run Q12
	0.066	Step edge 3	Transition flow	Run Q4
	0.064	Step edge 3	Transition flow	Run Q13
	0.058	Step edge 3	Transition flow	Run Q14
	0.052	Step edge 3	Transition flow	Run Q15
	0.046	Step edge 3	Transition flow	Run Q16
Series 2				Double-tip probe
	0.182	Step edge 6	Skimming flow	Run Q23.
	0.114	Step edge 5	Skimming flow	Run Q21.
	0.058	Step edge 3	Transition flow	Run Q22.

The flow rate was delivered by a pump controlled with an adjustable frequency AC motor drive, enabling an accurate discharge adjustment in a closed-circuit system. The discharge was measured from the upstream head above crest with an accuracy of about 2% (ACKERS et al. 1978, BOS 1976). Clear-water flow depths and velocities were measured with a point gauge and a Prandtl-Pitot tube (∅ =

3.3 mm) respectively. Air-water flow properties were measured using two types of conductivity probe: a single-tip probe (∅ = 0.35 mm), and a double-tip probe (∅ = 0.025 mm). The probe sensors were aligned in the flow direction and excited by an air bubble detector (AS25240). (The velocity measurements were the longitudinal component of the air-water interfacial velocity.) The probe signal was scanned at 5 kHz for 180 s and at 20 kHz for 20 s for the single-tip and double-tip probes respectively. The translation of the probes in the direction normal to the channel invert was controlled by a fine adjustment travelling mechanism connected to a Mitutoyo™ digimatic scale unit (Ref. No. 572-503). The error on the vertical position of the probe was less than 0.025 mm. The accuracy on the longitudinal position of the probe was estimated as $\Delta x < +/- 0.5$ cm. The accuracy on the transverse position of the probe was less than 1 mm. Flow visualisations were conducted with a digital video-camera Sony™ DV-CCD DCR-TRV900 (speed: 25 fr/s, shutter: 1/4 to 1/10,000 s) and high-speed still photographs.

Air-water flow properties were recorded for nineteen flow rates ranging from 0.046 to 0.182 m^3/s (Table 2-1). Measurements were conducted at the step edges, unless indicated (Fig. 2-1). Note that uniform equilibrium flow conditions were not achieved at the downstream end of the chute because the flume was relatively short. Full details of the experimental results are given in Appendix I.

3. Basic flow patterns

3.1 Flow regime

The facility was designed to operate with flow conditions ranging from nappe to skimming flow regimes (Fig. 3-1). For $d_C/h < 0.53$, where d_C is the critical depth and h is the step height, the water flowed down the chute as a succession of clear, distinct free-falling nappes (i.e. nappe flow regime). (Nappe flows were not specifically investigated. Relevant references include HORNER (1969) and CHANSON (1995a).) For $d_C/h > 0.97$, the flow skimmed over the pseudo-bottom formed by the step edges : i.e., skimming flow regime. Intense cavity recirculation was observed at each and every step. For intermediate discharges ($0.53 < d_C/h < 0.97$), a transition flow pattern was observed. Dominant flow features of transitions flows included strong splashing and droplet ejections at any position downstream of the inception point of free-surface aeration. Small to medium air cavities were observed irregularly. For example, a step with a small air pocket could be followed by a medium-size air cavity at the

downstream step, followed by a tiny air cavity at the next drop. For an observer standing on the bank, the transition flow had a chaotic appearance with irregular droplet ejections that were seen to reach heights of up to 3 to 5 times the step height. It did not have the quasi-smooth free-surface appearance of skimming flows, nor the distinctive succession of free-falling nappes observed in nappe flows.

With both transition and skimming flows, the upstream flow was non-aerated and the free-surface exhibited an undular profile of same wave length and in phase with the stepped invert profile. Free-surface instabilities were however observed (Fig. 3-2). Similar wave instabilities were discussed by ANWAR (1993) and CHANSON (1997b). ANWAR suggested that free-surface aeration may be initiated by free-surface wave development, while CHANSON showed experimental evidence of free-surface aeration in partially-developed flows.

The location of the inception of free-surface aeration was clearly defined for each and every test. (Experimental observations are reported in Table 2-1 & Appendix I.) Cavity aeration was typically observed one to two steps upstream of the inception point (Fig. 3-2). A similar observation was reported by HORNER (1969), CHAMANI (2000) and MATOS (2000).

Fig. 3-1 - Views of the experimental test section
(A) Skimming flow ($d_C/h = 1.5$) - Flow from left to right

(B) Transition flow ($d_c/h = 0.7$) - Photograph with high shutter speed (1/2,000 sec.)

Fig. 3-2 - Flow patterns next to the inception point of free-surface aeration
(A) Free-surface instabilities upstream of the inception point of free-surface aeration
Skimming flow, looking downstream ($d_c/h = 1.16$)

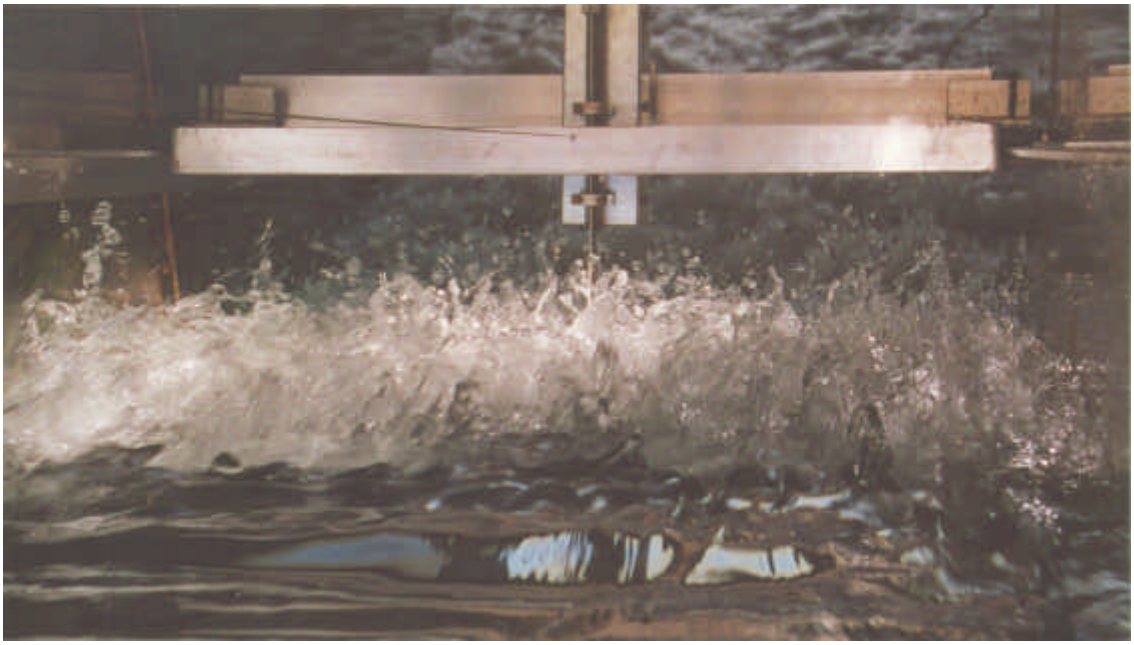

(B) Cavity aeration at the inception point of free-surface aeration (Courtesy of M. EASTMAN)
Transition flow, flow direction from the left to the right ($d_C/h = 0.6$) - Note the small air cavity

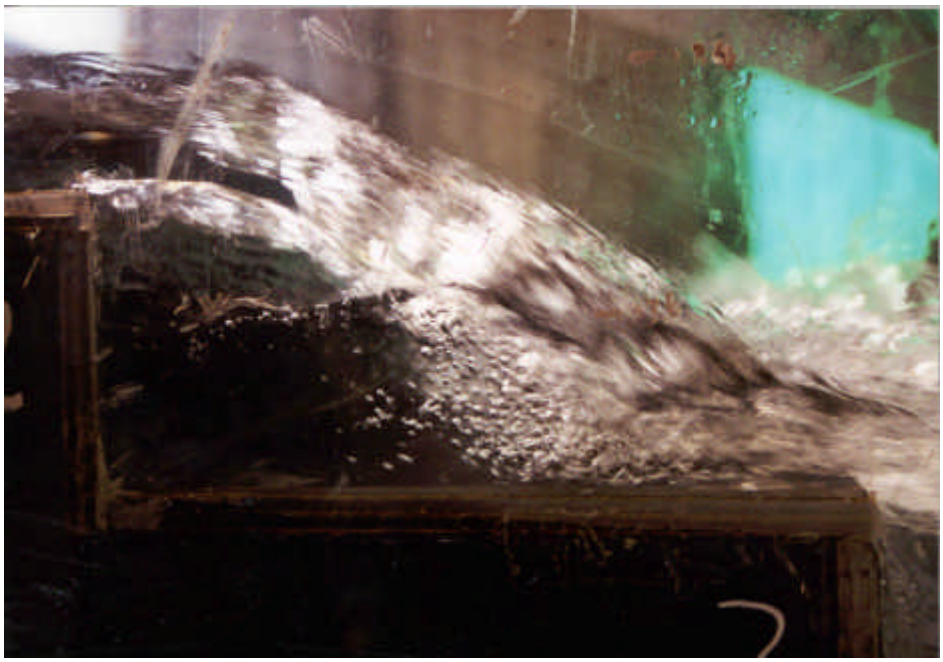

OHTSU and YASUDA (1997) were the first to mention the existence of a distinct "transition flow" regime (between nappe and skimming flows). The present observations of changes in flow regime are close to their findings : i.e., $0.78 < d_C/h < 1.05$ for $\alpha = 18.4^o$ (YASUDA and OHTSU 1999). These are further consistent with previous reviews of nappe-to-skimming flow transition conditions (e.g. RAJARATNAM 1990, CHANSON 1996).

3.2 Cavity recirculation in skimming flows

In skimming flows, intense three-dimensional cavity recirculation was observed at each step for all flow rates (Table 2-1). The recirculation vortices were best observed next to and downstream of the inception point, where entrained air bubbles within the step cavity enhanced visualisation. The skimming flows were characterised by unsteady momentum exchanges between the main stream and cavity flows. The recirculating fluid, at irregular time intervals, flowed outward into the main flow and was replaced by fresh fluid (Fig. 3-3). The ejection mechanism appeared sequential. Once one cavity outflow occured, it induced a sequence of outflows at the downstream cavities. Figure 3-3 illustrates the sequential fluid ejection in three successive step cavities. (The time scale between the upper and lower sketch is typically very short.) A similar pattern was documented with skimming flows past strip

roughness ([1]) while the sequential fluid ejection process was observed on the M'Bali stepped spillway model by Professor LEJEUNE, and at Nihon University by Professor OHTSU and Dr YASUDA. This is discussed in Appendix II.

Energy considerations show that the average fluid ejection frequency F_{ej} is proportional to the dimensionless boundary shear stress, and that the average outflow velocity is about half of the fluid inflow velocity (Appendix II). For a wide chute with flat horizontal steps, the dimensionless cavity ejection frequency is of the order of magnitude of :

$$\frac{F_{ej} * (h*\cos\alpha)}{U_w} \sim \frac{f}{5} \qquad (3\text{-}1)$$

where U_w is the main flow velocity, f is the Darcy friction factor, h is the step height and α is the slope of the pseudo-invert formed by the step edges. The duration of fluid ejection (or burst) must be smaller than the average ejection period. This yields a limiting condition in terms of flow resistance : $f \leq 1$. Larger flow resistance implies that the flow energy is dissipated by further means other than viscous dissipation in the cavity recirculation.

4. Air-water flow properties in skimming flows

Basic air-water flow properties

Downstream of the inception point of free-surface aeration, a rapid free-surface aeration was observed. Air concentration distributions, measured at step edges, exhibited a smooth continuous profile. Experimental results are presented in Figure 4-1 and compared with an analytical solution of the air bubble advective diffusion equation :

$$C = 1 - \tanh^2\left(K'' - \frac{\frac{y}{Y_{90}}}{2 * D_o} + \frac{\left(\frac{y}{Y_{90}} - \frac{1}{3}\right)^3}{3 * D_o} \right) \qquad \text{Skimming flows} \quad (4\text{-}1)$$

where y is distance measured normal to the pseudo-invert, Y_{90} is the characteristic distance where C = 90%, K" is an integration constant and D_o is a function of the mean air concentration C_{mean} only (App. III).

---

[1]Rectangular cavity : DJENEDI et al. (1994), ELAVARASAN et al. (1995). Triangular cavity : TANTIRIDGE et al. (1994).

Fig. 3-3 Sketch of sequential fluid ejections
From top to bottom : successive cavity ejections (burst and outflow) in three adjacent cavities

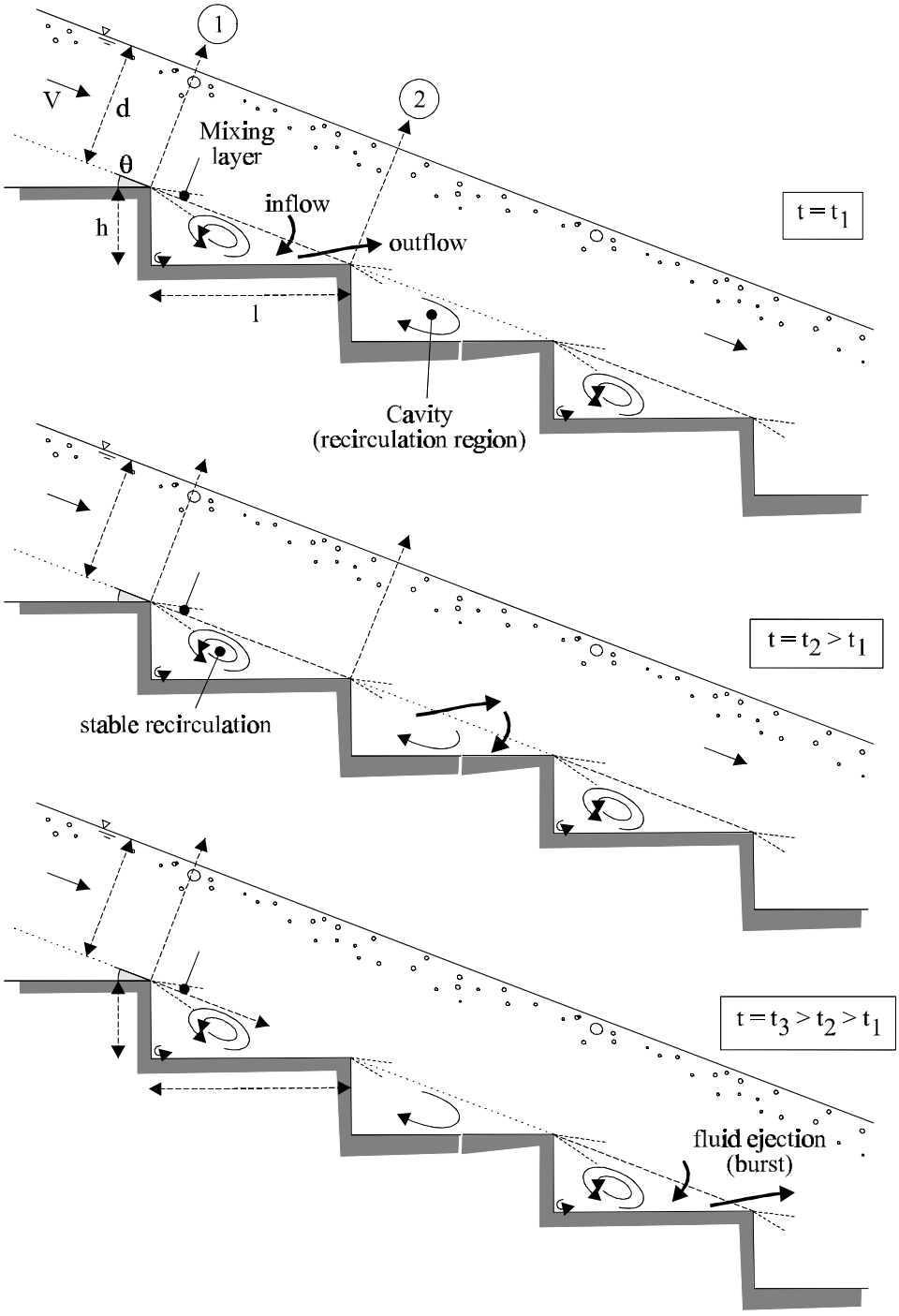

A small number of measurements were taken half-distance between two step edges (e.g. Fig. 4-1A). The results suggest consistently a greater overall aeration than at adjacent step edges, with some aeration of the fluid layers next to the recirculation cavity (i.e. $y/Y_{90} < 0.3$).

Velocity distributions measurements were performed at step edges (Fig. 4-1A). The results follow a

power law :

$$\frac{V}{V_{90}} = \left(\frac{y}{Y_{90}}\right)^{1/N} \qquad (4\text{-}2)$$

where V_{90} is the characteristic velocity for C = 90%. N was found to be about 5.1 and 6 for $d_c/h = 1.5$ and 1.1 respectively. MATOS (2000) performed air-water velocity measurements in a longer chute and he observed N ~ 4. CHANSON (1995a) found N = 3.5 and 4 for the earlier works of FRIZELL (1992) and TOZZI (1992) respectively.

In the present study, the flume was relatively short and uniform equilibrium flow conditions were not achieved. This might account for some difference with MATOS' results.

Figure 4-1C presents dimensionless distributions of bubble count rates $F_{ab}*d_c/V_c$, where F_{ab} is the bubble frequency, d_c is the critical depth and V_c is the critical flow velocity. For a given flow velocity and void fraction, the bubble count rate F_{ab} is inversely proportional to the mean bubble size, and directly proportional to the air-water specific interface area (e.g. CHANSON 1997c). The relationship between the bubble frequency and air content exhibits a characteristic parabolic shape which is best fitted by :

Fig. 4-1 - Air-water flow properties in skimming flows
(A) Experimental data for $Q_W = 0.182$ m^3/s - Comparison with Equations (4-1) and (4-2)
Inception of free-surface aeration upstream of step edge 6

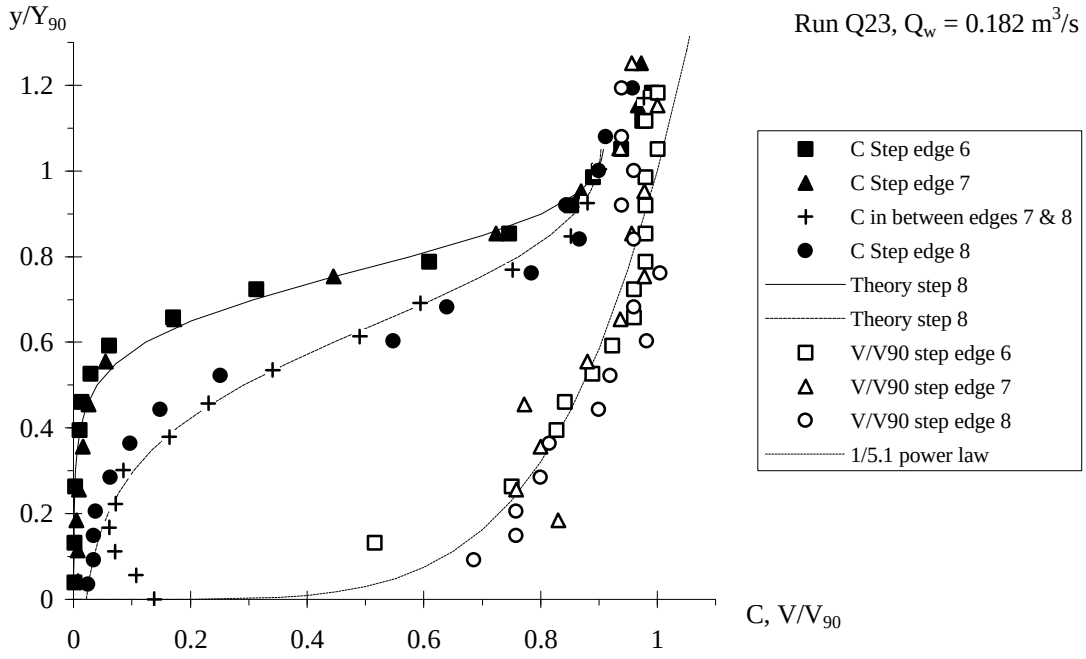

(B) Experimental data for Q_W = 0.147 m^3/s - Comparison with Equation (4-1)
Inception of free-surface aeration upstream of step edge 5

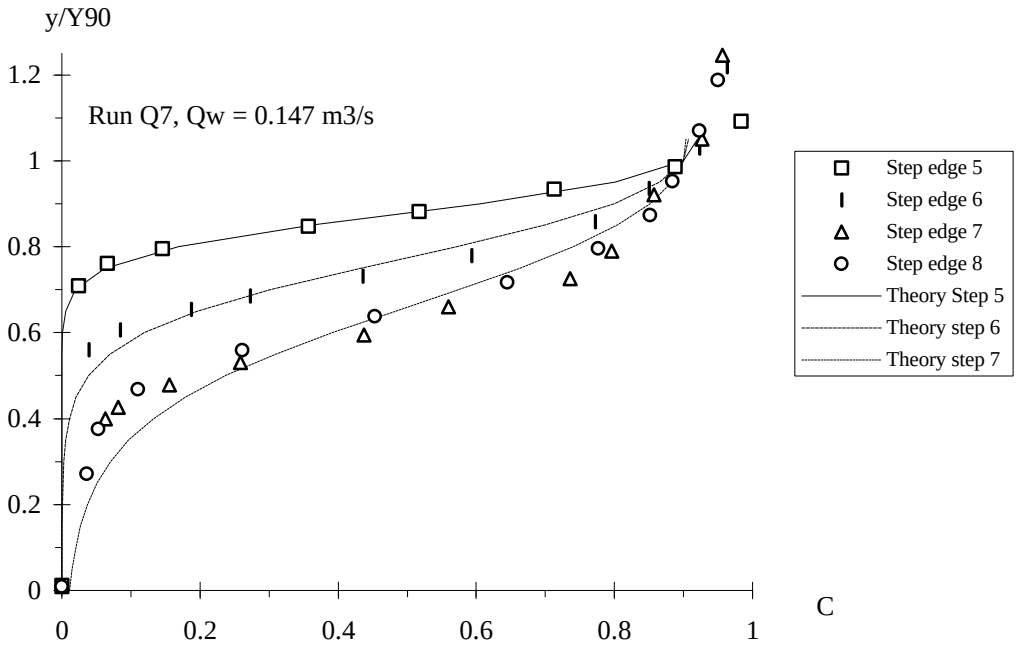

(C) Dimensionless bubble count rate distributions (data measured with single-tip probe) for Q_W = 0.147 m^3/s

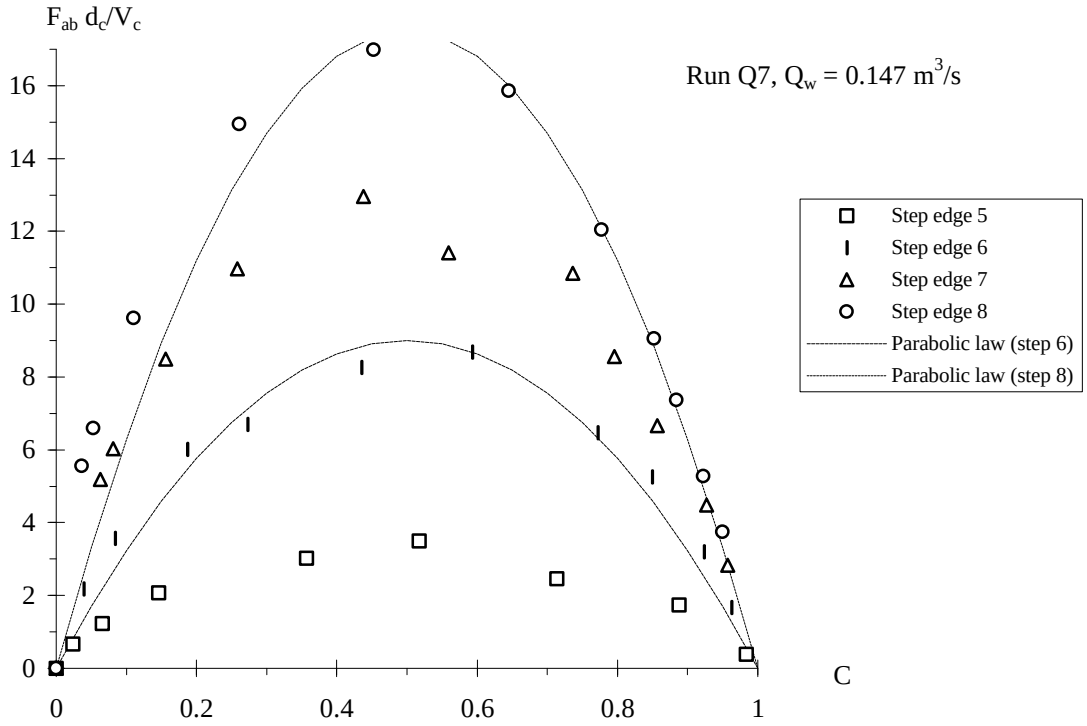

$$\frac{F_{ab}}{(F_{ab})_{max}} = 4 * C * (1 - C) \quad (4\text{-}3)$$

where the maximum bubble frequency $(F_{ab})_{max}$ is seen for about C ~ 50%.

Bubble and droplet chord length data

Measured chord length size distributions are presented in Figure 4-2. Each figure shows the normalised chord length probability distribution function where the histogram columns represent the probability of a bubble chord length in 0.5 mm intervals : e.g., the probability of a chord length from 2.0 to 2.5 mm is represented by the column labelled 2.0. The last column (i.e. > 20) indicates the probability of bubble chord lengths larger than 20 mm. Air bubble chord length distributions are in white and water droplet chord length distributions are in black. The data give some information on the characteristic sizes of air bubbles and water droplets. They show the broad spectrum of bubble and droplet chord lengths observed at each location : i.e., from less than 0.5 mm to larger than 20 mm (Fig. 4-2). Results from both the bubbly flow region (C < 0.3 to 0.4) and the splashing region (0.6 to 0.8 < C) are shown.

The air bubble chord length distributions are skewed with a preponderance of small bubble sizes relative to the mean. The probability of bubble chord lengths is the largest for bubble sizes between 0 and 1.5 mm for C ≈ 0.1 and between 0 and 2.5 mm for C ≈ 0.2. It is worth noting the large fraction of bubbles larger than 20 mm for C ≈ 10 and 20%. These might be large air packets surrounding water structures. For completeness, the fraction of bubbles larger than 20 mm was significantly higher between step edges, possibly as the results of cavity aeration.

Although water droplet chord length distributions appeared skewed with a preponderance of small drop sizes relative to the mean, the distributions differ from bubble chord length distributions for similar liquid and void fractions respectively, indicating consistently larger droplet chord lengths (Fig. 4-2). A similar result was noted in smooth-invert chute flow (CHANSON 1999a).

Dimensionless specific interface area distributions were calculated. Results are presented in Appendix I in terms of the depth-averaged specific interface area a_{mean}. Experimental results show maximum specific interface areas up to 650 m^{-1}, with depth-average mean specific area ranging from 20 to 310 m^{-1} (App. I). For all skimming flow experiments, greater specific interface areas were measured in between step edges than at the adjacent step edges. It is believed that the aeration of the recirculation

flow contributes even further to the interface area ([2]).

Fig. 4-2 Bubble and droplet chord length distributions (white = air bubbles - black = water droplets)
(A) Void and liquid fractions : 10% (Q_W = 0.182 m^3/s)

	Y_{90} (m)	C_{mean}	$(F_{ab})_{max}$ (Hz)
Step edge 7	0.070	0.23	110
between step edges 7 and 8	0.090	0.40	123
Step edge 8	0.088	0.38	132

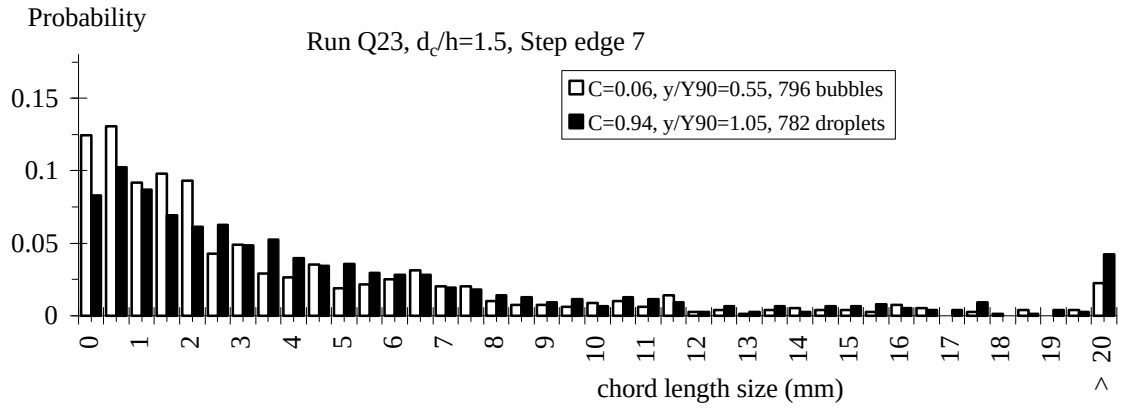

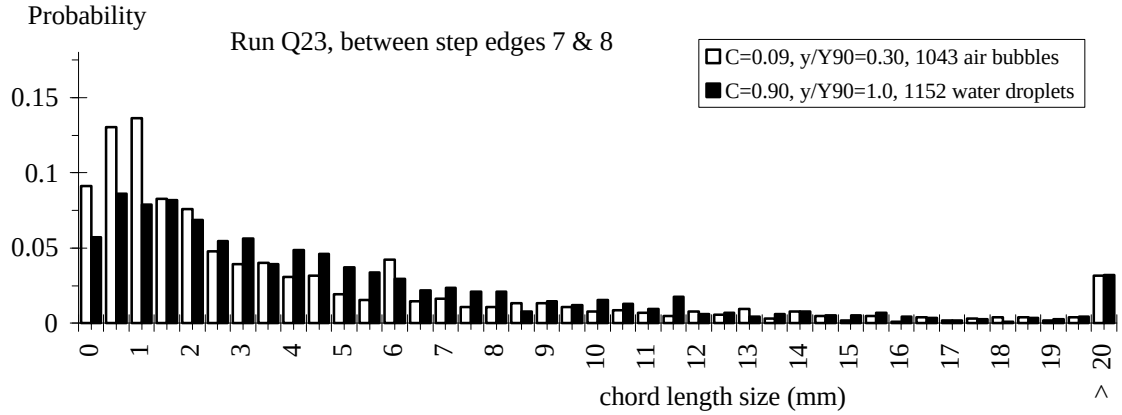

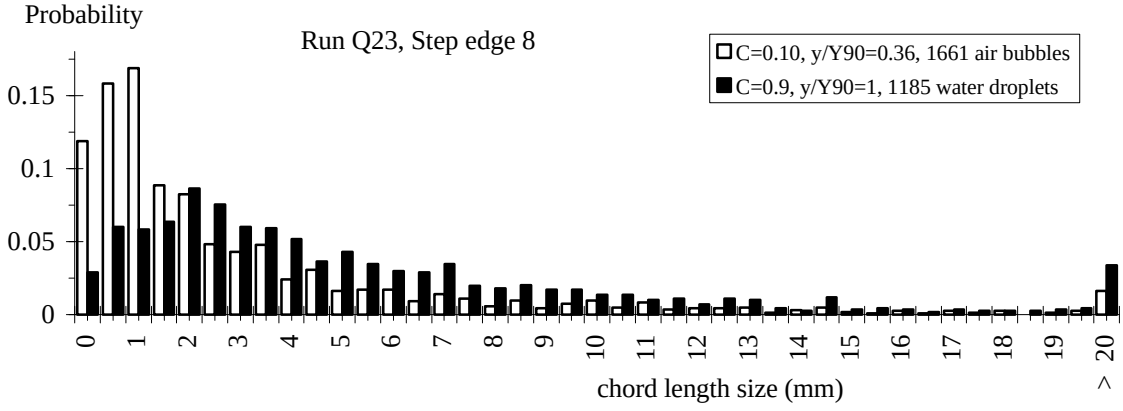

[2]No measurement was conducted in the recirculation cavity (y <0) to avoid probe tip damage.

(B) Void and liquid fractions : 20% (Q_W = 0.114 m^3/s)

	Y_{90} (m)	C_{mean}	$(F_{ab})_{max}$ (Hz)
Step edge 7	0.065	0.43	258
between step edges 7 and 8	0.070	0.53	205
Step edge 8	0.060	0.43	283

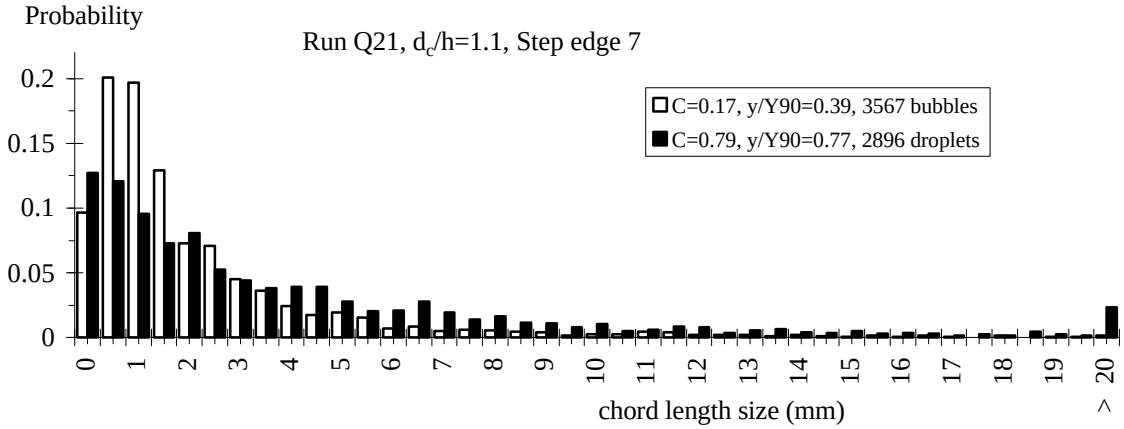

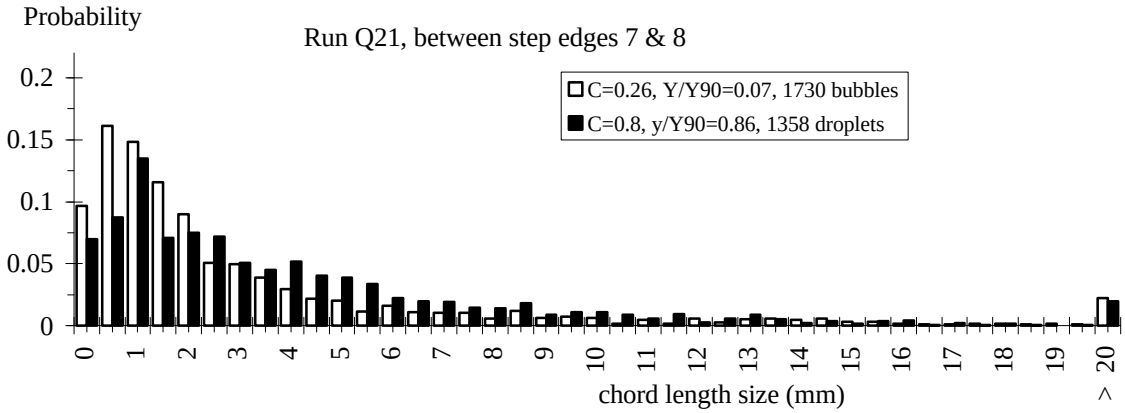

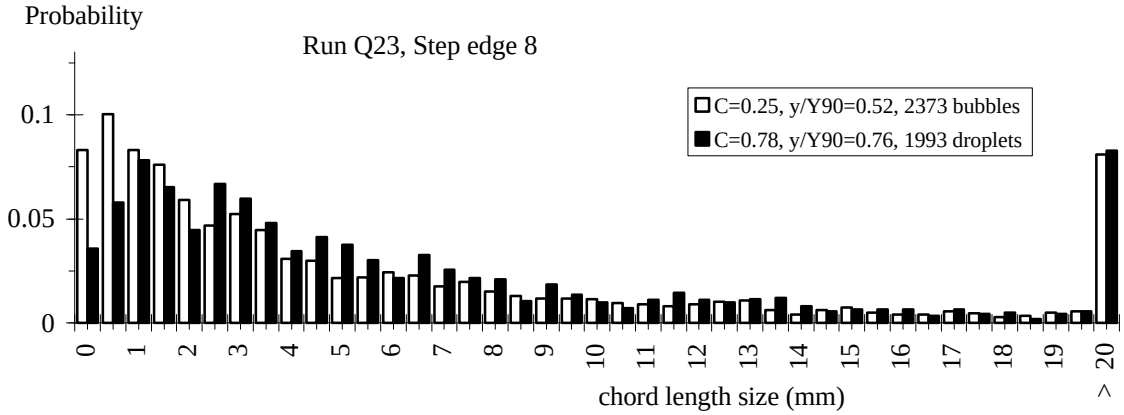

Turbulent velocity field

Distributions of time-averaged air-water velocity V and modified turbulence intensity Tu' are presented

in Figure 4-3. The data were measured with a dual-tip resistivity probe and details of the processing technique are given in Appendix IV. Although Tu' is not exactly equal to the turbulence intensity, it provides some qualitative information on the turbulence level in the flow. Figure 4-3B includes data measured at step edges (white symbols) and in between step edges (black symbols).

In Figure 4-3 the distributions of turbulence intensity Tu' exhibit relatively uniform profiles implying high turbulence levels across the entire air-water flow mixture (i.e. $0 \leq y \leq Y_{90}$). The trend differs significantly from well-known turbulence intensity profiles observed in turbulent boundary layers (e.g. SCHLICHTING 1979). On stepped chutes, it is believed that the high rate of energy dissipation, associated with form drag, contributes to strong turbulent mixing throughout the entire flow. Greater turbulence levels are expected within the developing shear layers : i.e. in the wake of each step edge. Despite some scatter, the trend is observed for the lower regions ($y/Y_{90} < 0.2$ to 0.3) (Fig. 4-3B).

Although the quantitative values of turbulence intensity Tu' are large (~ 100%), they are of the same order of magnitude as turbulence levels measured in separated flows past rectangular cavity (HAUGEN and DHANAK 1966, Fig. 9), in wakes between large stones (SUMER et al. 2001) and in the developing shear region of plunging water jets (CHANSON and BRATTBERG 1998).

Fig. 4-3 - Dimensionless velocity and turbulent intensity distributions in skimming flow
(A) q_W = 0.182 m^2/s, step edge 8

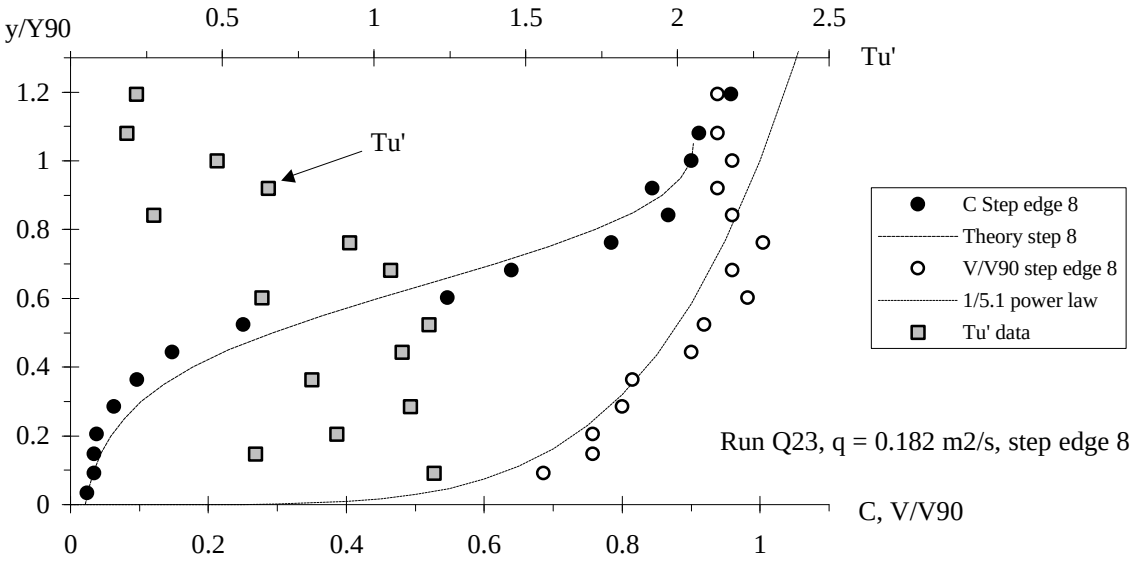

(B) Turbulent intensity distributions at step edges and in between step edges (q_W = 0.182 m^2/s)

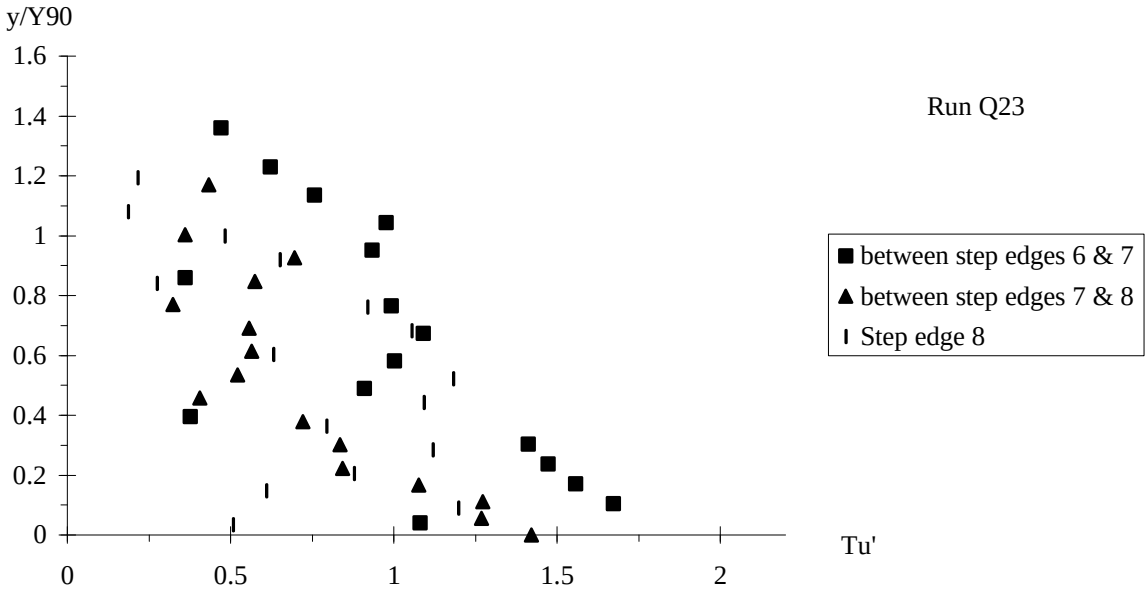

Comparison of void fraction profiles between smooth- and stepped-invert chute flows

Although the distribution of air concentration follows a trend similar to that seen in smooth-invert chute flows, small differences were consistently observed. This is highlighted in Figure 4-4 with a comparison of void fraction distributions obtained for identical mean air concentration. Black symbols are prototype smooth-invert chute data (CAIN 1978, Aviemore dam spillway) and the cross symbols are stepped chute data (Present study). The skimming flow data are compared with Equation (4-1) while smooth chute data are compared with CHANSON's (1995b) model developed and validated for smooth chute flows :

$$C = 1 - \tanh^2\left(K' - \frac{y/Y_{90}}{2 * D'}\right) \qquad \text{Self-aerated flows} \quad (4\text{-}4)$$

where the integration constant K' and the dimensionless air bubble diffusivity D' are functions of the mean air content only (App. III).

The comparison of void fraction profiles indicates that, for an identical mean air content, skimming flows are more aerated in the upper flow layer (C > 0.3 to 0.5) than in smooth-invert self-aerated flows, and lesser air is observed in the lower layers (Fig. 4-4). A similar trend was observed with the stepped chute data of TOZZI et al. (1998). The result suggests a stronger droplet ejection mechanism in skimming flows, whereby water ejections reach comparatively higher elevations (than in smooth chute flows) before re-attaching to the flow. The trend may be related to different turbulent processes: i.e.,

skin friction in smooth-invert chutes versus form drag in skimming flow down stepped chutes.

Fig. 4-4 - Comparison of air concentration distributions in smooth-invert and stepped chute flows
Smooth-invert data : black symbols, solid line (Eq. (4-4))
Stepped chute date : cross symbols, dashed line (Eq. (4-1))
(A) C_{mean} = 0.27

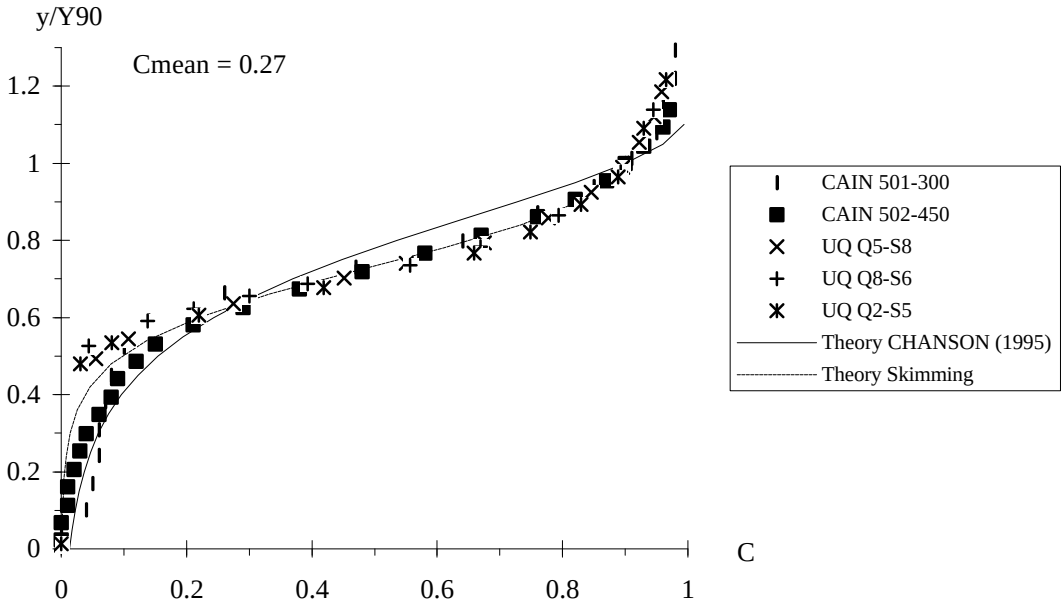

(B) C_{mean} = 0.35

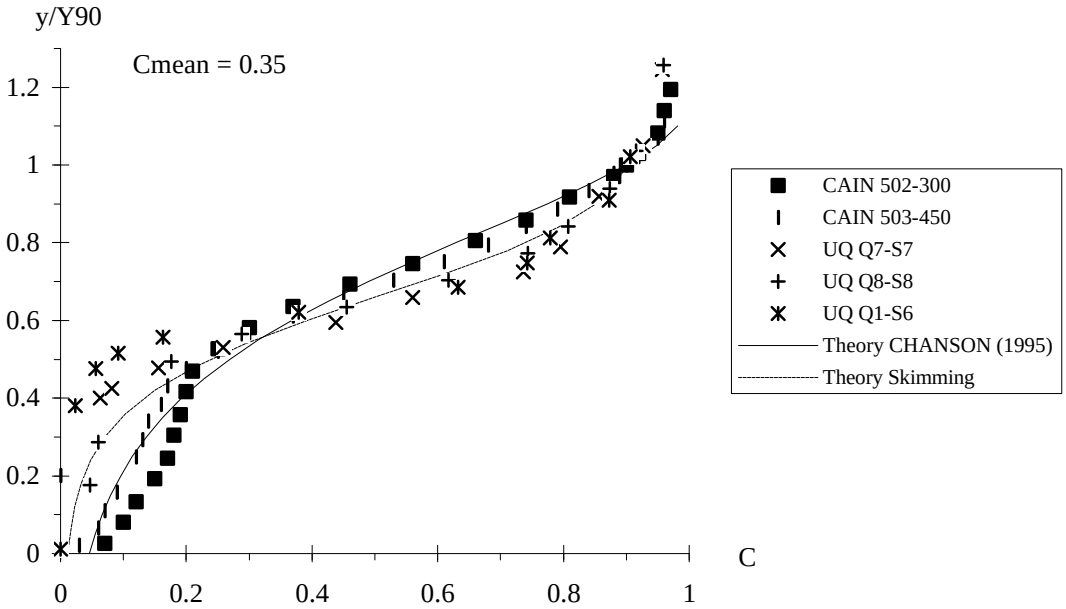

5. Air-water flow properties in transition flows

Free-surface aeration was found to be very intense for all transition flow rates (Table 2-1, App. I). Downstream of the inception point of free-surface aeration, mean air concentrations ranged from 0.2 to 0.6 typically, with maximum mean air content of up to 78% measured at one step edge. Major redistributions of air content and velocity were observed between adjacent, successive step edges. Similar longitudinal fluctuations of flow properties were observed in transition flows down a 3.4º stepped chute (h = 0.071 and 0.143 m) (CHANSON 2001), suggesting that the finding is not specific to the facility. Figure 5-1 shows air-water flow properties for one typical flow rate.

At most step edges, the distributions of air concentration may be fitted by :

$$C = K''' * \left(1 - \exp\left(- \lambda * \frac{y}{Y_{90}}\right)\right) \qquad \text{Transition flows} \quad (5\text{-}1)$$

where K''' and λ are function of the mean air content only (App. III). Equation (5-1) compares favourably with most data, except for the first step edge downstream of the inception point of free-surface aeration and for the deflecting jet flow (e.g. Fig. 5-1).

For most flow rates, a deflecting flow was observed a few steps downstream of the inception point of free-surface aeration. Visually, the flow appeared to bypass one step, barely touching the step edge. At that step, liquid fractions (1-C) greater than 10% were measured at distances up to $1.5*d_c$ and some spray overtopped the 1.25-m high sidewalls. The nappe re-attached the main flow at the next downstream step. In Figure 5-1A, such a deflected nappe is seen at the 6th step edge. (Further locations of deflected nappe are reported in Appendix I.)

In transition flows, the distributions of bubble count rates follow about the parabolic law (Eq. (4-3)) that was observed in smooth-invert chute flows and in skimming flows (Fig. 5-1B).

Turbulent velocity field

Air-water velocity distributions are presented in Figure 5-2 in terms of the time-averaged air-water velocity V and a modified turbulence intensity Tu' (Appendix IV). The distributions of turbulence intensity Tu' exhibit relatively uniform profiles across the air-water flow mixture (i.e. $y \leq Y_{90}$). The quantitative values of turbulence intensity Tu' are comparable with skimming flow data (Fig. 4-3).

The writers note that, in a transition flow, the shape of the air concentration profiles is nearly identical

for a given flow rate, while the velocity distributions are rapidly varied from step edge to step edge.

Discussion

Equation (5-1) is an analytical solution of the diffusion equation (App. III). It assumes that the air bubble diffusivity is zero for C = 0 and C = 1, and that it follows a distribution :

$$D' = \frac{C * \sqrt{1 - C}}{\lambda * (K' - C)} \qquad (5\text{-}2)$$

The shape is somehow similar to the sediment diffusivity distribution developed by ROUSE (1937), leading to the Rouse distribution of suspended matter.

In a transition flow, the design of the sidewalls must account for the deflecting jet flows. That is, the chute sidewall height must be sized to at least $Y_{90} \sim 1.6*d_c$, or even larger than $1.4*Y_{90} = 2.2*d_c$ if splashing is not acceptable : e.g., with a road next to the spillway chute and high risks of frost and icy conditions. For comparison, Y_{90}/d_c was found to be less than 0.7 to 0.8 in skimming flows, during the present study (Fig. 6-1A).

Fig. 5-1 - Experimental results in a transition flow
Q_W = 0.058 m^3/s - Comparison with Equation (5-1) - Inception point upstream of the step edge 3
(A) Air concentration and velocity distributions

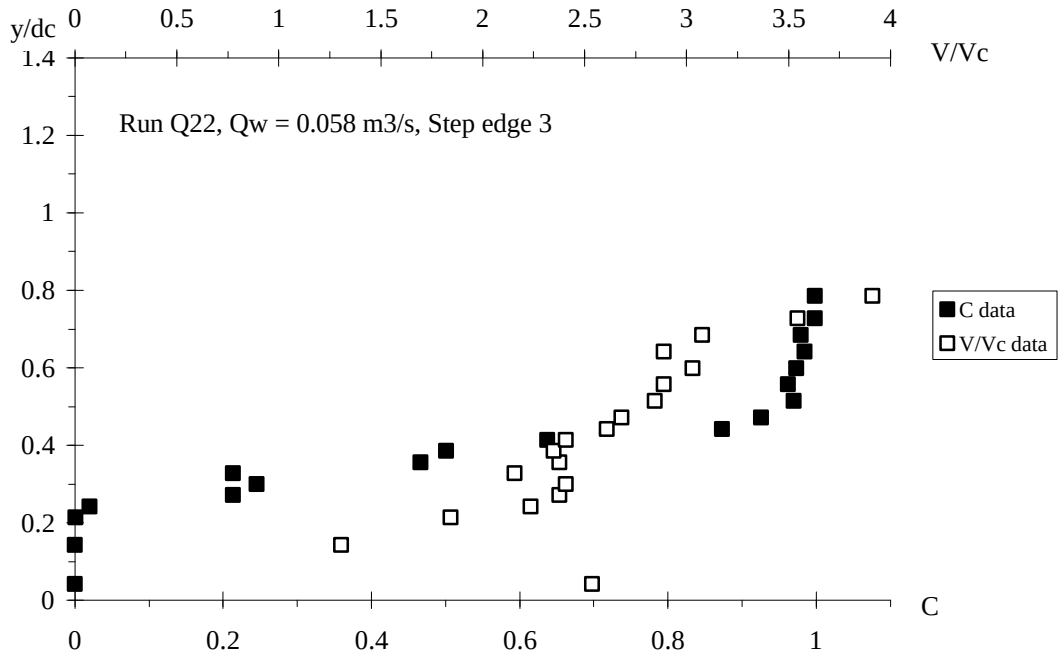

(A) Air concentration and velocity distributions

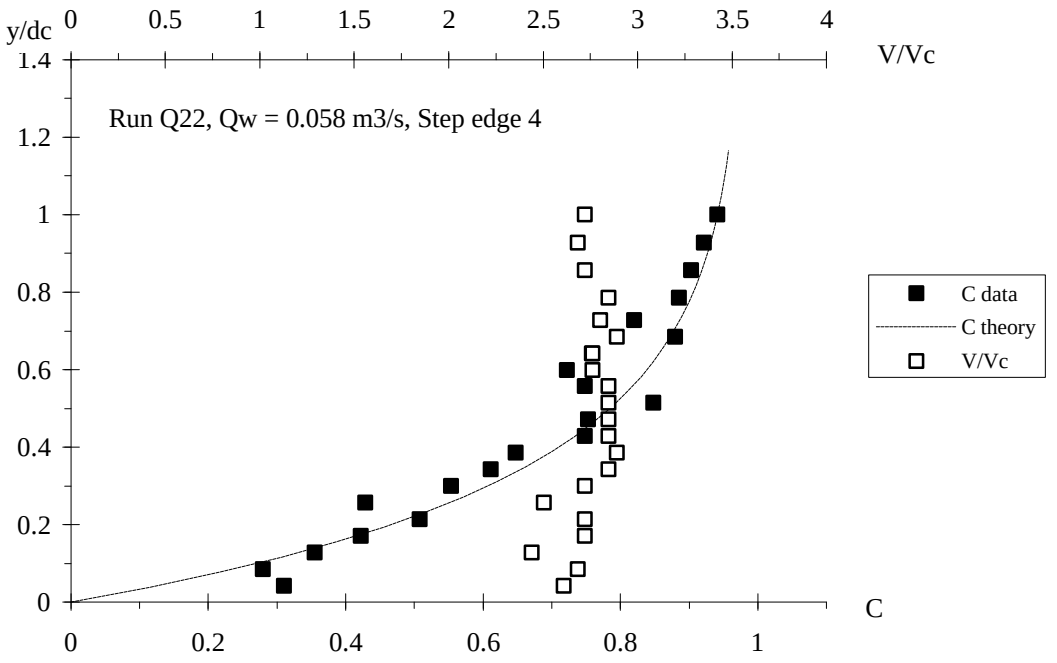

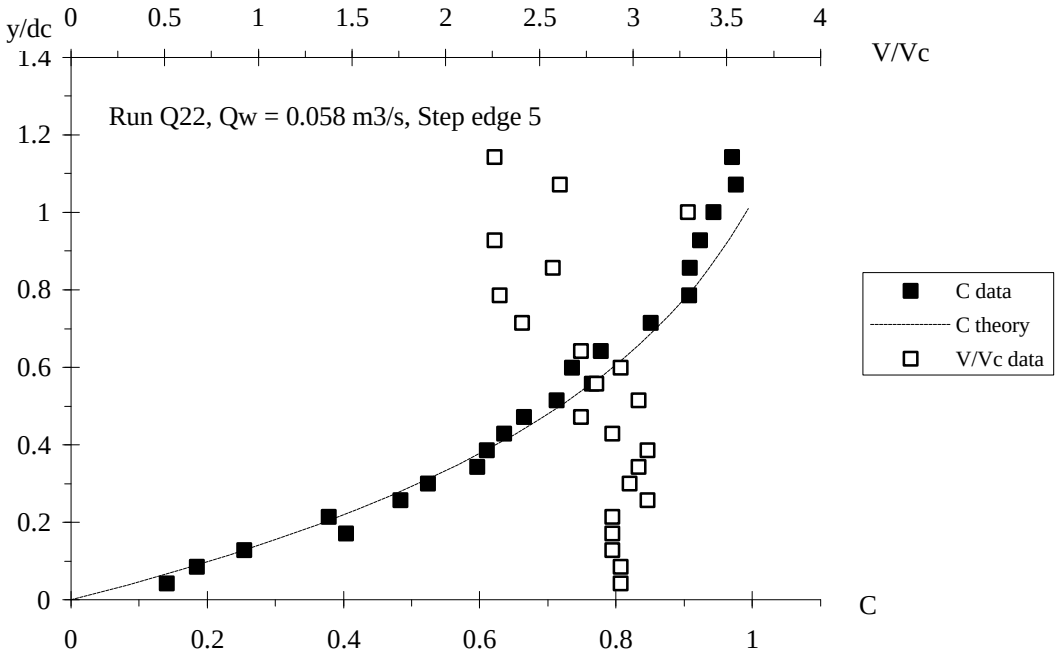

(A) Air concentration and velocity distributions

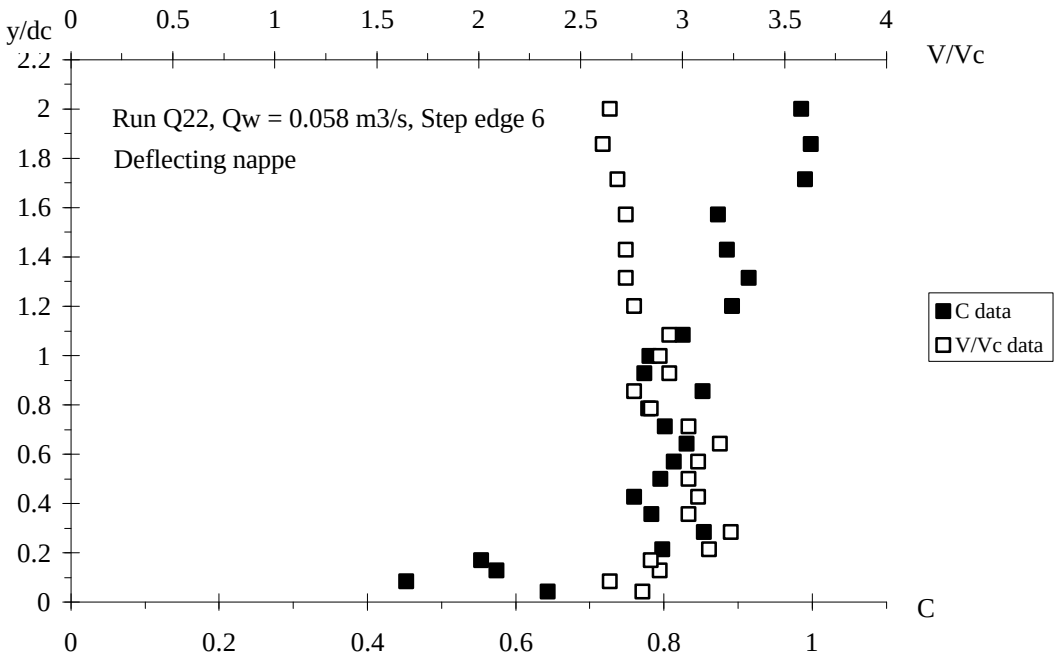

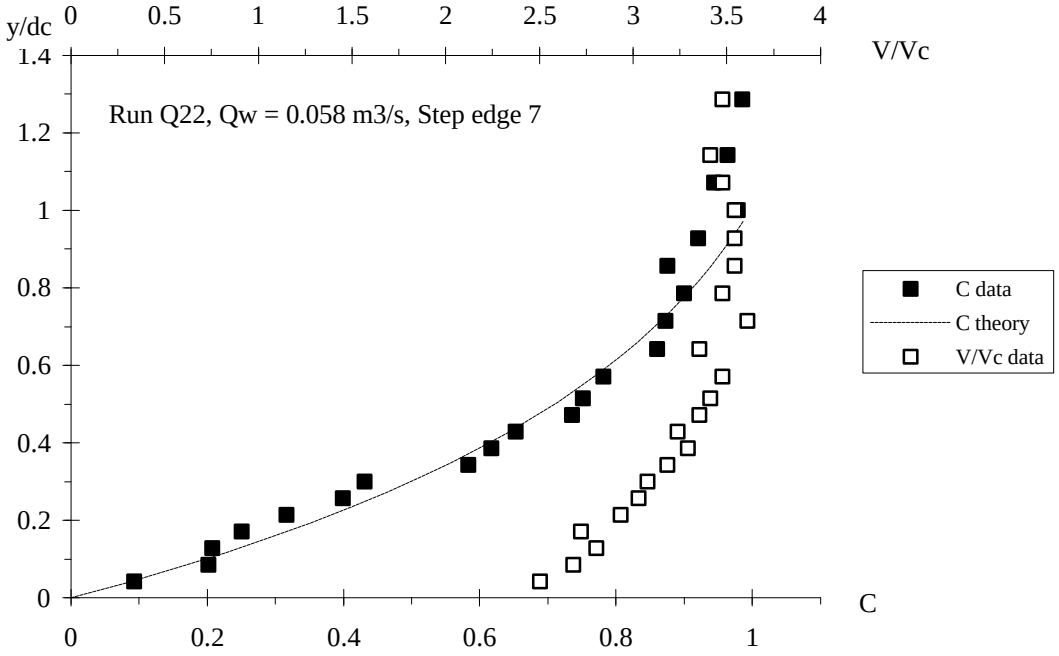

(A) Air concentration and velocity distributions

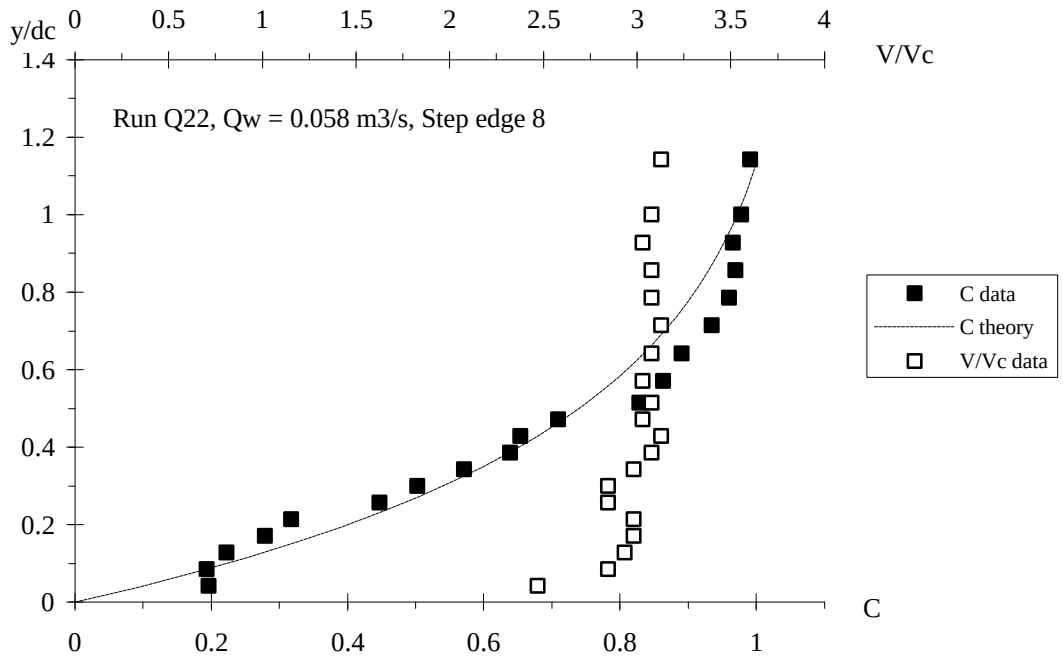

(B) Dimensionless bubble count rate distributions

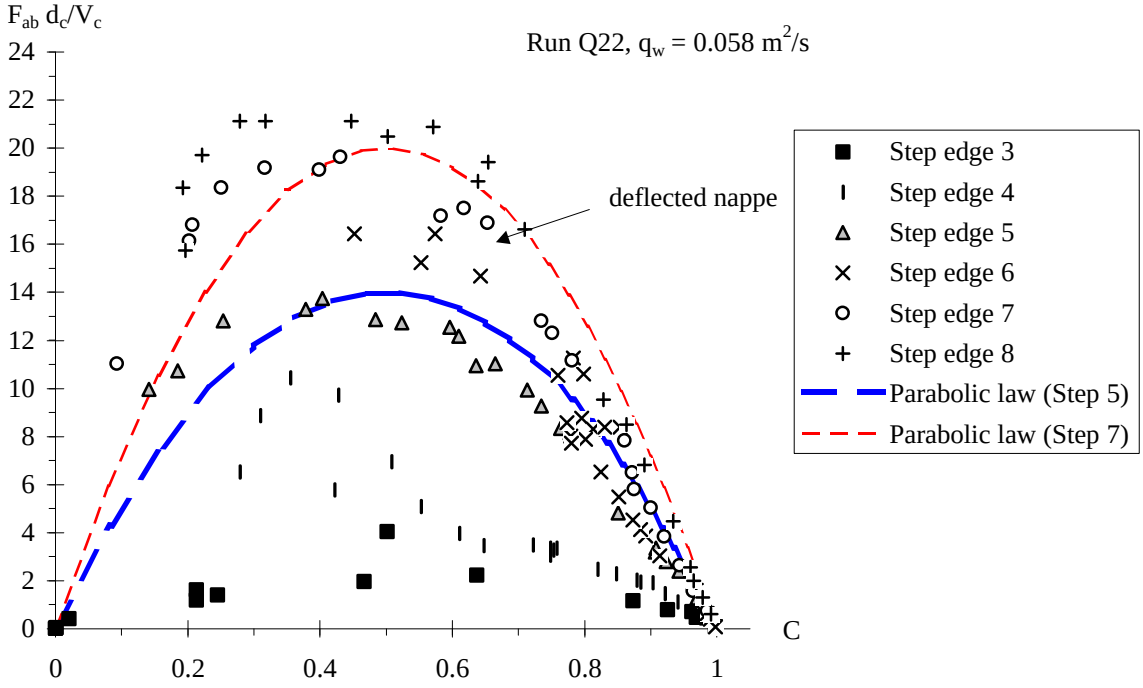

Fig. 5-2 - Dimensionless velocity and turbulent intensity distributions in transition flow
Run Q22, q_W = 0.058 m^2/s, step edge 8

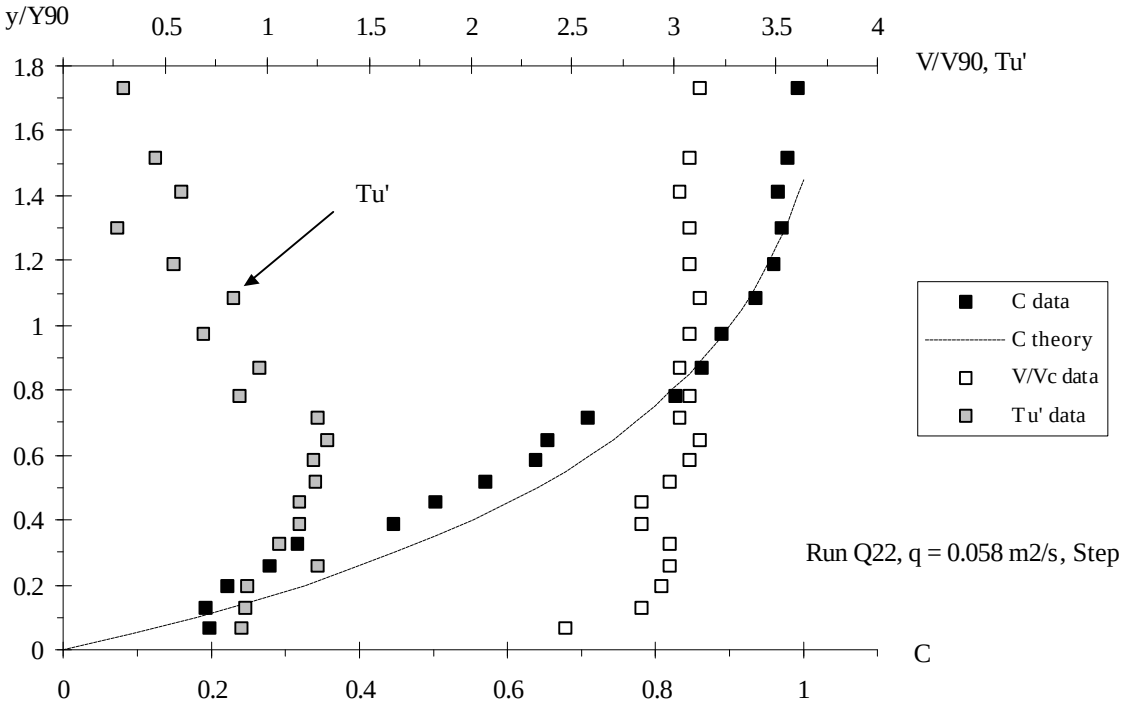

6. Discussion : air-water flow properties and flow resistance

6.1 Air-water flow properties

Longitudinal distributions of mean air concentration C_{mean} and dimensionless air-water depth Y_{90}/d_c are presented in Figure 6-1, where the horizontal axis s/d_c is the ratio of the distance from the downstream end of the broad crest to the critical depth. Note that the chute was relatively short and that uniform equiibrium flow conditions were not achieved at the downstream end.

In skimming flows, rapid aeration was observed at the inception point, followed by a gradual increase (Fig. 6-1A). In Figure 6-1A, the data are compared with the numerical model developed for smooth-invert chutes by WOOD (1985) and extended by CHANSON (1993b). Calculations were conducted assuming a friction factor f = 0.3.

Transition flow data are presented in Figure 6-1B. Note the different horizontal and vertical ranges between Figures 6-1A and 6-1B. Very large aeration was observed in transition flows, in excess of acknowledged limits observed in smooth chute flows (e.g. WOOD 1991, CHANSON 1997b,c). The air-water flow depth data Y_{90} exhibited a saw-edged pattern, reaching up to 1.4 to 1.6 times d_c at

deflected nappes. Overall both sets of curves do not show a monotonic trend. Rather chaotic, irregular variations with increasing distances from the crest were observed.

Fig. 6-1 - Longitudinal distributions of mean air content C_{mean} and dimensionless depth Y_{90}/d_c
(A) Skimming flow data - Comparison with numerical calculations (WOOD 1985, CHANSON 1993b)

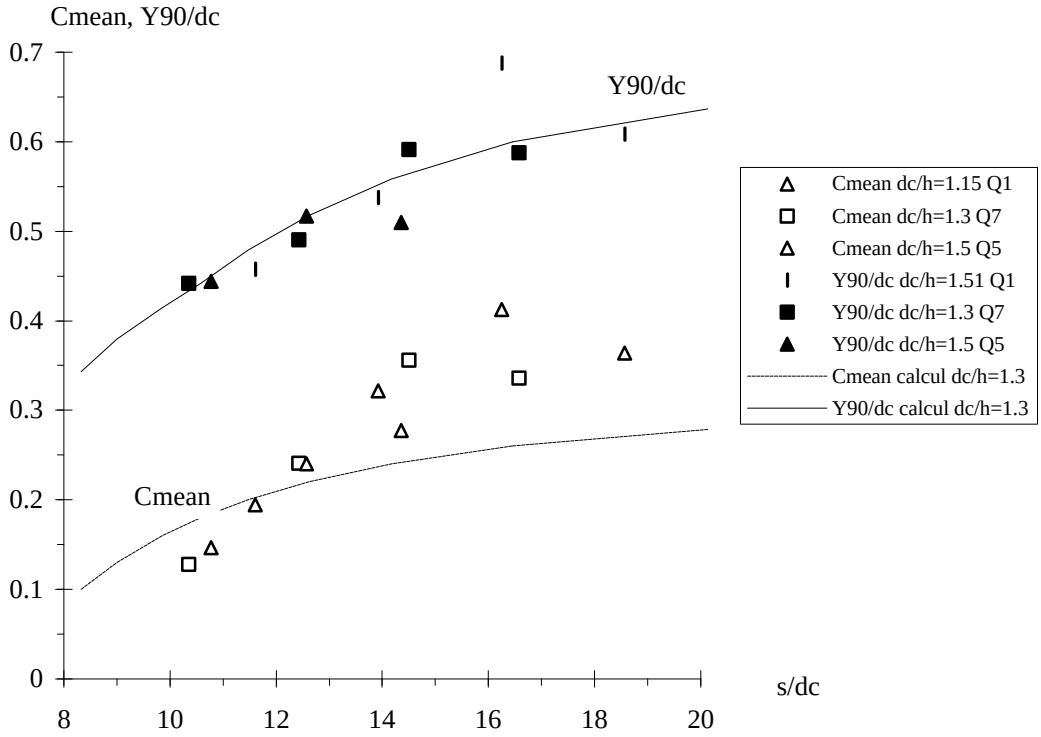

(B) Transition flow data

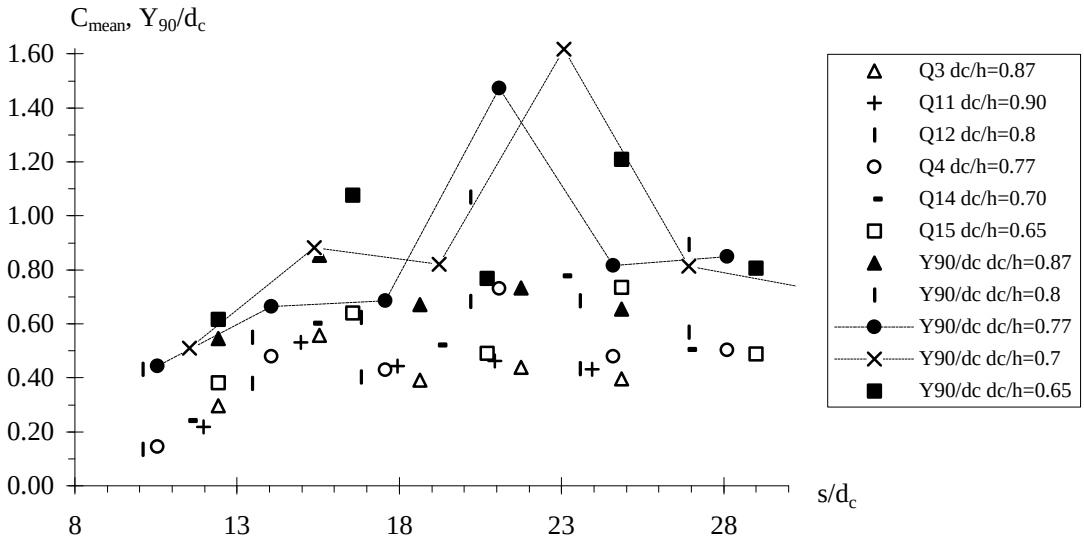

Similar instabilities were measured down a 3.4º stepped chute (h = 0.07 & 0.14 m) at the University of Queensland (CHANSON 2001). OHTSU and YASUDA observed also the chaotic nature of transition flows for slopes ranging from 5.7º to 55º, although it appeared more pronounced "cha os" for $\alpha < 35^o$ (Personal communication).

Experimental results show that the maximum bubble frequency $(F_{ab})_{max}$ increased with longitudinal distance for each and every flow rate, and that it did not reach an upper limit within the length of the experimental channel. The test section was indeed relatively short and uniform equilibrium was not achieved at the downstream end. Figures 4-1C and 5-1B illustrate the longitudinal increase in maximum bubble frequency for a skimming flow and a transition flow respectively.

6.2 Flow resistance in skimming flows

Skimming flows are characterised by significant form drag and form losses take place predominantly in the cavity recirculation (see section 3.2, App. II). In gradually-varied flows downstream of the inception point, the average shear stress between the skimming flow and the cavity recirculation may be calculated from the friction slope S_f ([3]). For a wide channel the energy equation yields:

$$f_e = \frac{8 * \tau_o}{\rho_w * U_w^2} = \frac{8 * g * \left(\int_{y=0}^{y=Y_{90}} (1 - C) * dy \right) * S_f}{U_w^2} \qquad \text{Gradually-varied flow (6-1)}$$

where the friction slope equals $S_f = - \partial H/\partial s$, H is the depth-averaged total head, s is the curvilinear coordinate along the flow direction, f_e is the Darcy friction factor for air-water flow, C is the local void fraction, y is measured normal to the pseudo-invert formed by the step edges, and U_w is the mean flow velocity ($U_w = q_w/d$). For the present series of experiments, the flow resistance was estimated using Equation (6-1) (Table 6-1). In Figure 6-2, the data are compared with experimental data obtained in large-size laboratory flumes : i.e., h > 0.02 m and Re > 1 E+5. All 166 data were re-analysed using the criteria of CHANSON et al. (2000).

0.30 (166 data) (Fig. 6-2B).

[3]The friction slope is the slope of the total head line (HENDERSON 1966, CHANSON 1999b).

Table 6-1 - Summary of experimental results of flow resistance in skimming flows

Ref.	Q_w m^3/s	Flow regime	f_e	Remarks
(1)	(2)	(3)	(3)	(4)
Series 1				Single-tip probe.
	0.182	Skimming flow	0.143	Run Q5
	0.164	Skimming flow	0.157	Run Q6
	0.147	Skimming flow	0.196	Run Q7
	0.130	Skimming flow	0.184	Run Q8
	0.124	Skimming flow	0.215	Run Q1
	0.114	Skimming flow	0.283	Run Q9
	0.103	Skimming flow	0.157	Run Q2
	0.099	Transition flow	0.158	Run Q10
Series 2				Double-tip probe.
	0.182	Skimming flow	0.092	Run Q23.
	0.114	Skimming flow	0.074	Run Q21.

Fig. 6-2 - Flow resistance in skimming flow: conditional analysis
(A) Steep stepped chute data ($\alpha > 20^o$) {166 data} - Comparison with Equation (6-2) ($f_d = 0.2$)
Laboratory data :

f_i (estimate neglecting air entrainment)	BaCaRa (1991), YASUDA and OHTSU (1999), SHVAINSHTEIN (1999)
f_e (based upon air-water flow properties)	CHAMANI and RAJARATNAM (1999), YASUDA and OHTSU (1999) (55º only), MATOS (2000), BOES (2000), Present study

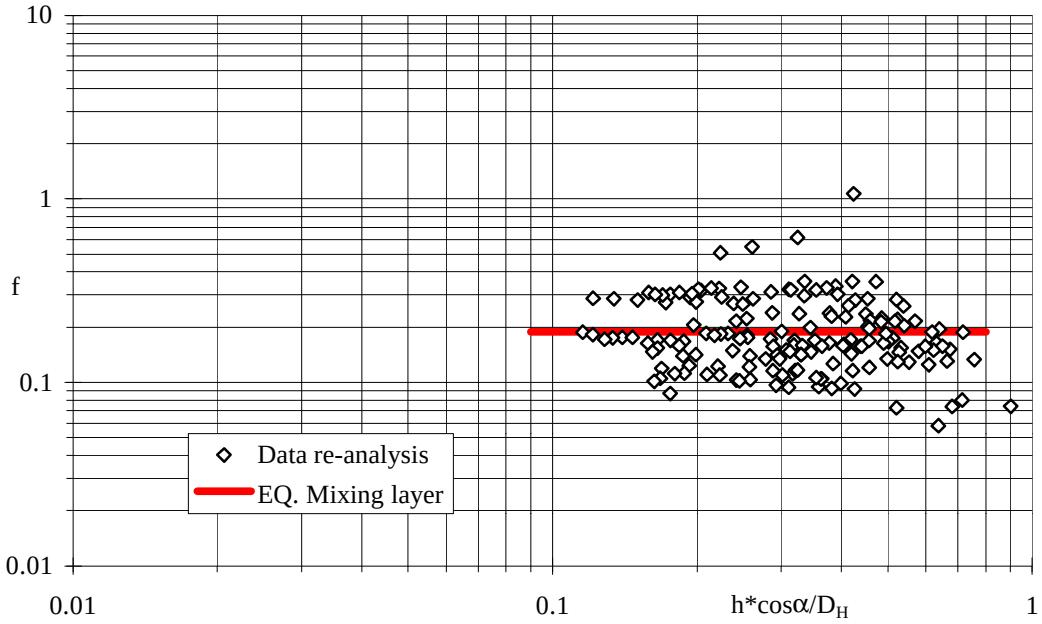

(B) Probability distribution function of steep chute friction factor ($\alpha > 20^o$) {166 laboratory data}

f_i (estimate neglecting air entrainment)	BaCaRa (1991), YASUDA and OHTSU (1999), SHVAINSHTEIN (1999)
f_e (based upon air-water flow properties)	CHAMANI and RAJARATNAM (1999), YASUDA and OHTSU (1999) (55° only), MATOS (2000), BOES (2000), Present study

Uncontrolled broad-crest	YASUDA and OHTSU (1999), Present study
Uncontrolled smooth ogee crest	CHAMANI and RAJARATNAM (1999)
Uncontrolled ogee crest, with small first steps in ogee development	BaCaRa (1991), SHVAINSHTEIN (1999), MATOS (2000)
Pressurised intake	BOES (2000)

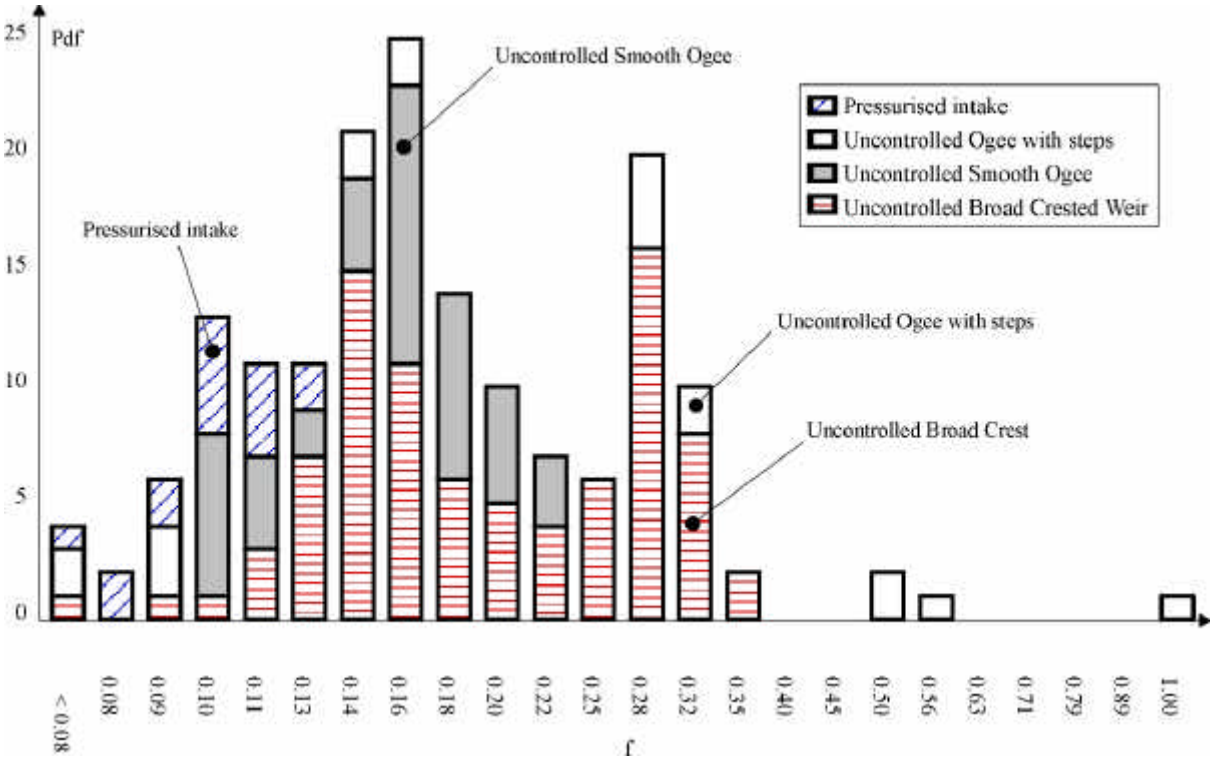

The friction factor data present no obvious correlation with the relative step roughness ($h*\cos\alpha/D_H$), Reynolds, Froude nor Weber numbers. However they compare favourably with a simplified analytical model of the pseudo-boundary shear stress which may be expressed, in dimensionless form, as :

$$f_d = \frac{8 * \tau_o}{\rho_w * U_w^2} = \frac{2}{\sqrt{\pi}} * \frac{1}{K} \qquad (6\text{-}2)$$

where f_d is an equivalent Darcy friction factor estimate of the form drag, 1/K is the dimensionless expansion rate of the shear layer (CHANSON et al. 2000). Equation (6-2) predicts $f_d \approx 0.2$ for K = 6 : i.e., close to the observed friction factors (Fig. 6-2A).

Figure 6-2B presents the probability distribution function of the Darcy friction factor where the

histogram columns represent the number of data with friction factors within the interval ([4]) : e.g., the probability of friction factors from 0.18 to 0.20 is represented by the column labelled 0.18. The first and last column indicates the number of data with friction factors less than 0.08 and greater than 1.0 respectively. The experimental data are distributed around three dominant values: f ≈ 0.105, 0.17 and 0.30 (166 data) (Fig. 6-2B).

Fig. 6-3 - Cavity recirculation, developing shear layer and re-attachment in skimming flows

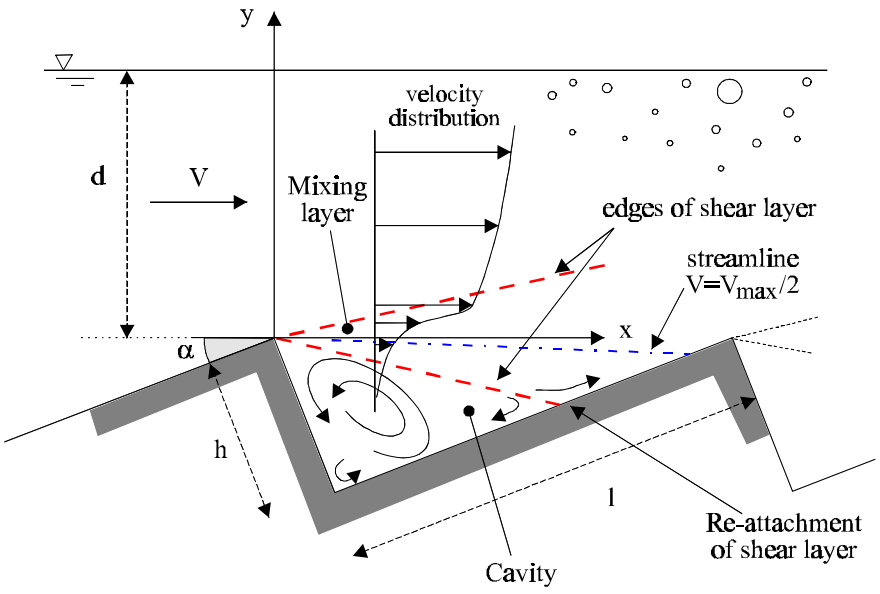

Discussion

The writers hypothesise that flow resistance in skimming flows (down steep slopes) is not an unique function of the flow rate and stepped chute geometry, but that the form drag process presents several modes of excitation. At each step edge, shear instabilities may develop in the shear layer (e.g. NAUDASCHER 1967) (Fig. 6-3). In turn, the instabilities could generate different cavity wake regimes, associated with different drag coefficients. In Figure 6-2B, the dominant values f ≈ 0.105, 0.17 and 0.30 are assumed to correspond to the three dominant modes (or regimes).

Different modes of excitation may be induced by different inflow conditions, affecting cavity recirculation processes in a cascading effect (i.e. sequential cavity ejections, Fig. 3-3). At the upstream

[4]The intervals were selected with a constant logarithmic increment

end, the inflow turbulence does affect the cavity recirculation and the distance to re-attachment of the shear layer (Fig. 6-3). In turn, this will affect all the stepped chute because of the sequential ejection process (Fig. 3-3). Figure 6-4 summarises basic inflow configurations. With an uncontrolled ogee profile, the pressure distribution is atmospheric in the entire flow at design flow conditions by definition of the ogee development (HENDERSON 1966, CHANSON 1999b) ([5]). The inflow pressure coefficient C_p is zero, where C_p is defined as :

$$C_p = \frac{1}{\frac{1}{2} * \rho * g * d^2} * \int_0^d P(y) * dy$$

With an uncontrolled broad-crest, the pressure is hydrostatic at the crest and $C_p = 1$. For a pressurised intake, the inflow pressure distribution is greater than hydrostatic (i.e. $C_p >> 1$).

Figure 6-2B shows that experiments with pressurised intake yield lower flow resistance than for uncontrolled inflow conditions. For example, the re-analysis of BOES' (2000) data gives $f \sim 0.1$: i.e., about three times smaller than the third dominant value. Skimming flow experiments at the University of Queensland down a flat slope ($\alpha = 3.4^o$, $h = 0.07$ m) yielded friction factors $f \sim 0.03$, that are three times smaller than data of YASUDA and OHTSU (1999) ($f \sim 0.08$) on a 5.7^o stepped slope ($h = 0.025$ & 0.05 m) with uncontrolled broad-crest.

The type of excitation mode (or regime) may further be affected by the cavity dimensions (ratio h/l), cavity aeration (greater aeration are likely on steep slopes), and compliance of the stepped invert (construction material) which could lead to different vibration regimes. There is some analogy with form drag behind bluff bodies. For the flow behind a cylinder, the drag coefficient is known to be a function of the upstream turbulence affecting the boundary layer separation for a given Reynolds number ([6]). For ventilated cavities behind wedges and wings, several regimes were associated with different drag coefficients for the same inflow conditions, depending upon the amount of ventilation (SILBERMAN and SONG 1961, LAALI and MICHEL 1984, MICHEL 1984, VERRON and

---

[5]A further sub-division may be made between an entire smooth ogee profile and an ogee development with small first steps in the profile (Fig. 6-3).

[6]For infinitely long smooth cylinders, the effect is best observed for Reynolds numbers about 1 E+5 to 1 E+6.

MICHEL 1984).

The above results may further be influenced by drag reduction associated with air bubble entrainment (section 6.3).

Fig. 6-4 - Definition sketch of inflow conditions

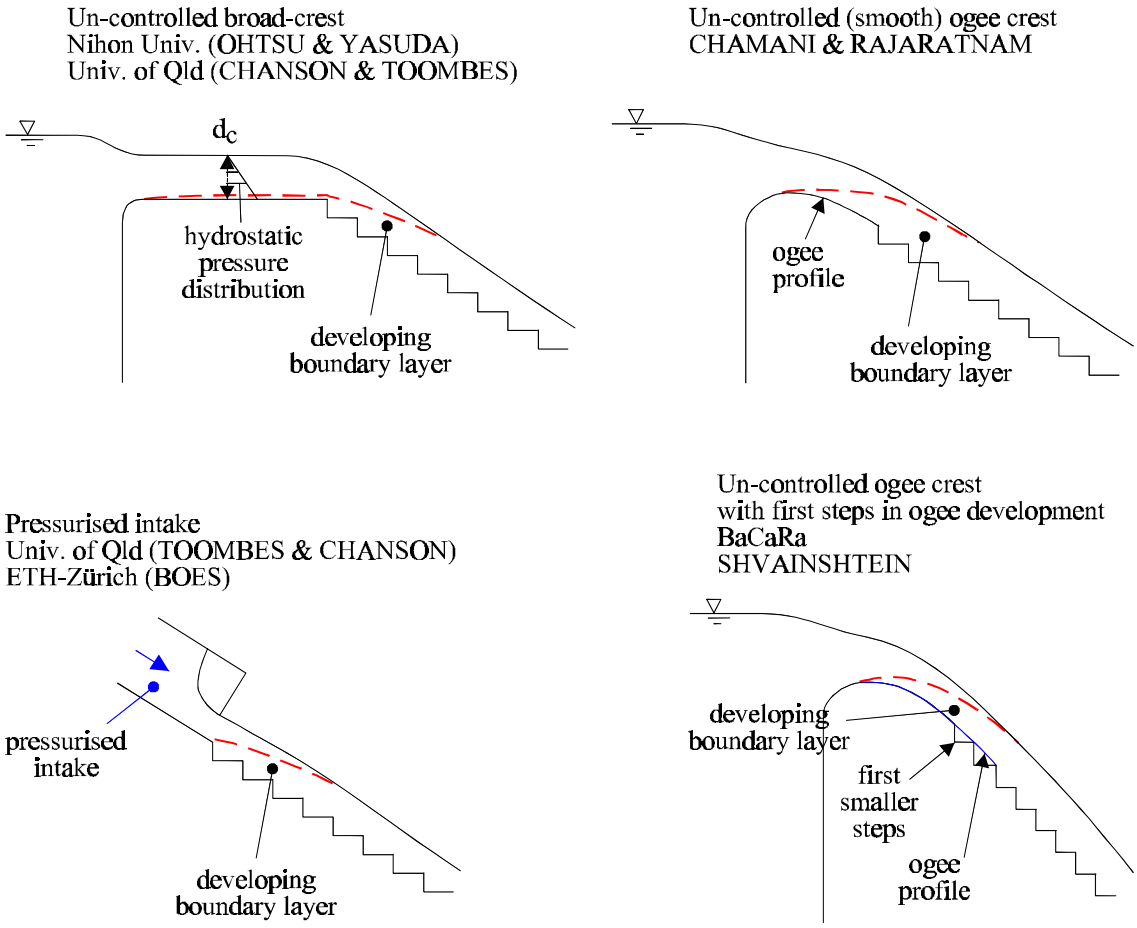

6.3 Drag reduction in skimming flows

On smooth-invert chutes, the presence of air within turbulent boundary layers reduces the shear stress between flow layers, and hence the shear force (WOOD 1983, CHANSON 1994). An estimate of the drag reduction is :

$$\frac{f_e}{f} = 0.5 * \left(1 + \tanh\left(0.628 * \frac{0.514 - C_{mean}}{C_{mean} * (1 - C_{mean})}\right)\right) \qquad \text{Smooth chute (6-3)}$$

where tanh is the hyperbolic tangent function, C_{mean} is the mean air concentration, f is the clear-water friction factor and f_e is the Darcy friction factor of air-water flow (CHANSON 1994). Equation (6-3)

characterises the reduction in skin friction associated with air entrainment causing a thickening of the momentum sublayer (CHANSON 1994,1997b).

The re-analysis of detailed air concentration measurements in skimming flows shows a decrease in friction factor f_e with increasing mean air concentration (Fig. 6-5, Table 1-1). The re-analysed stepped chute data are best correlated by :

$$\frac{f_e}{f_d} = 0.5 * \left(1 + \tanh\left(0.68 * \frac{0.5 - C_{mean}}{C_{mean} * (1 - C_{mean})}\right)\right) \qquad \text{Skimming flow (6-4)}$$

where f_d is the dimensionless pseudo-boundary shear stress for clear-water flow (Eq. (6-2)). Equation (6-4) is compared with experimental data in Figure 6-5 assuming a mixing layer expansion rate : 1/K = 0.22 (Eq. (6-2)). Equation (6-3) is also shown. Despite some scatter, the results confirm CHANSON's assumption that a drag reduction process caused by air entrainment occurs on stepped spillways (CHANSON 1993a,1995a). The trend (Eq. (6-4) is very close to drag reduction estimate on smooth-chutes (Eq. (6-3)) although the drag reduction mechanism is entirely different (Fig. 6-5).

In skimming flows, separation occurs at each step edge and a shear layer develops with cavity recirculation beneath (Fig. 3-3 & 6-3). It is believed that drag reduction results from interactions between the entrained bubbles and the developing mixing layer. Small air bubbles tend to resist stretching and this leads to some vortex inhibition. Hydrodynamic interactions between bubbles affect their orientation in the flow and might play a key role in reducing the instability of the flow as with fibre addition in water flows (e.g. AZAIEZ 2000). Interactions between particles and turbulent structures were visualised in developing shear layers of dilute polymer solutions, showing the existence of large-scale turbulent structures and a drastic reduction in number of small-scale eddies with polymer additives (e.g. RIEDIGER 1989).

Fig. 6-5 - Drag reduction in skimming flows - Comparison between Equations (6-3) and (6-4), and laboratory data

f_e (based upon air-water flow properties)	CHAMANI and RAJARATNAM (1999), YASUDA and OHTSU (1999) (55º only), MATOS (2000), BOES (2000), Present study

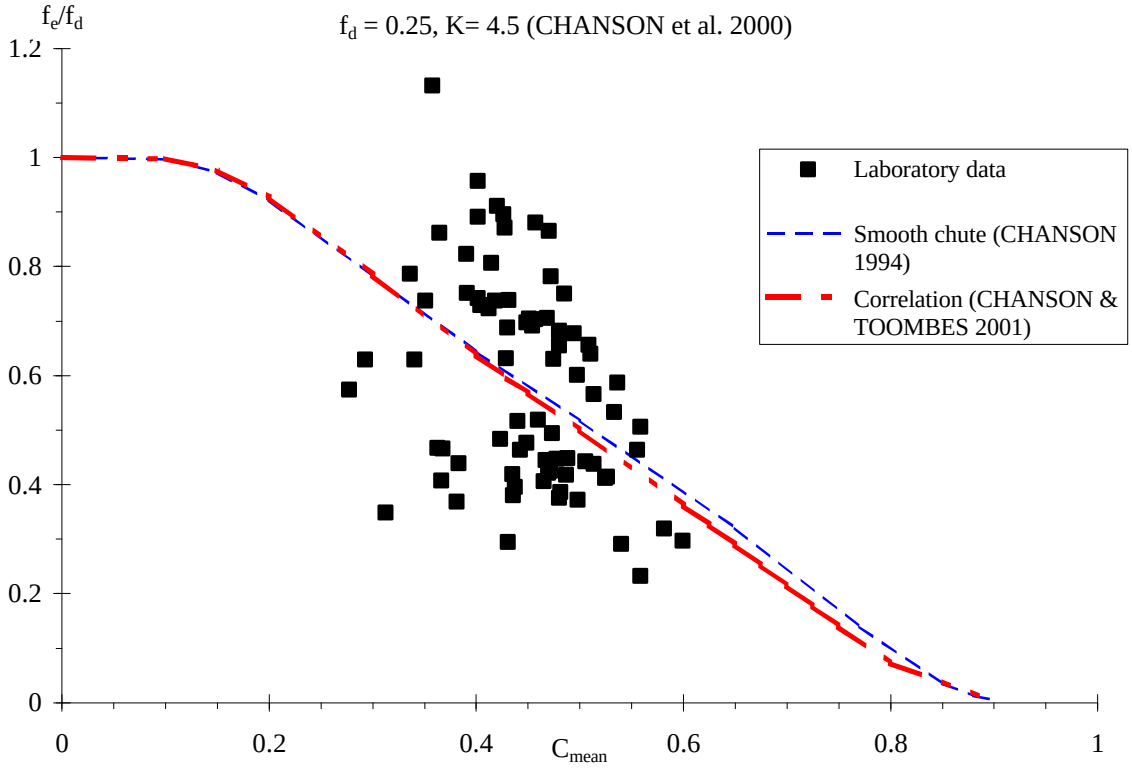

Part II - Hydraulic design of embankment overflow stepped spillways

7. Embankment overflow stepped spillways

Flood protection of an embankment dam is usually achieved by combining a side spillway of relatively large capacity with a reservoir storage "buffer" (i.e. empty volume) for flood attenuation. In recent years, the design floods of a number of dams were re-evaluated and the revised flows were often larger than those used for the original designs. In many cases, occurrence of the revised design floods would result in dam overtopping because of the insufficient storage and spillway capacity of the existing reservoir. Embankment overtopping is not acceptable because the rushing waters would scour the embankment slope leading to the rapid and total failure of the embankment.

Some overflow systems were developed in Australia : e.g., flow through rockfill embankment (e.g. OLIVIER 1967), the minimum energy loss weir design (e.g. Chinchilla weir, TURNBULL and McKAY 1974), the concrete slab chute system at Crotty rockfill dam (Tasmania). Although technically successful, these designs are not often economical. Recently new flood protection systems were introduced, allowing controlled embankment overtopping over a reinforced downstream stepped slope. Basic reinforcement techniques include concrete overtopping protection, precast concrete blocks, timber cribs, sheet-piles, riprap and gabions, and reinforced earth.

Concrete overtopping protection

Concrete overtopping protection allows an increase of spillway capacity. In North-America, a number of dam overtopping rehabilitations were conducted primarily on embankment structures with dam heights ranging from 4.6 to 33.5 m. It is believed that the first ones were the Ocoee No. 2 timber crib dam in 1980 and the Brownwood Country Club earth dam in 1984. Various construction techniques were used. Current trends favour the use of roller compacted concrete (RCC) ([7]) (Fig. 7-1).

[7]RCC dam rehabilitation accounted for nearly two-thirds of the RCC dam construction in USA in the 1990s.

Fig. 7-1 - Concrete overflow protection system for embankments
(A) Sketch of an overflow protection system with roller compacted concrete

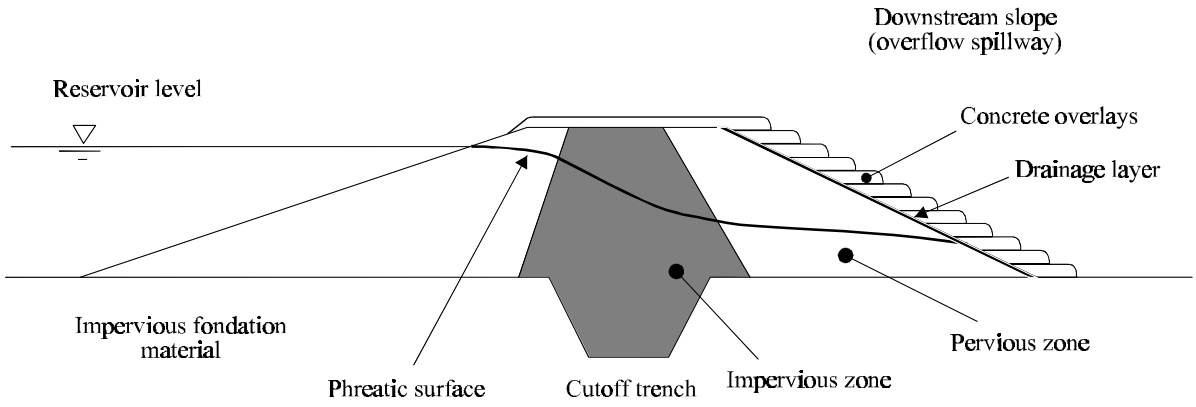

(B) Construction of a RCC spillway for detention basin West of Las Vegas, designed by the US Corps of Engineers

Roller compacted concrete is placed in a succession of overlays of 0.2 to 0.4-m thickness and with a width greater than 2.5 m for proper hauling, spreading and compacting. Exposed RCC is frequently used for secondary spillways with infrequent spills of less than 5 m^2/s. Alternatively, a conventional concrete protection overlay may be applied after the RCC or at the completion of construction works to

protect the RCC. With both RCC and conventional concrete protection, a drainage system beneath the concrete layers is essential to prevent uplift. Its purpose is to relieve pore pressure at the interface between the embankment and RCC overlays. In some cases, the drainage installation may be replaced or supplemented with drain holes formed through the RCC during placement. At the downstream end a cutoff wall must be built to prevent undermining of the concrete layer during overtopping.

Precast concrete steps

Soviet engineers were among the first to propose a stepped concrete chute design on the downstream face of embankment dams under the leadership of P.I. GORDIENKO (CHANSON 1995a, 2001) (Fig. 7-2). The choice of a stepped structure allows the use of individual blocks interlocked with the next elements and the design assists in the energy dissipation. The design concept was more recently tested in USA and UK, although it did not prove cost-effective there. An interesting feature of the concrete block system is the flexibility of the stepped channel bed allowing differential settlements of the embankment.

Fig. 7-2 - Earth dam stepped spillway with precast concrete blocks : Sosnovsky farm dam (Russia, 1980) (Courtesy of Prof. Y. PRAVDIVETS) - H = 11 m, design flow : 3.3 m^2/s, $\alpha = 10^o$, W = 12 m, overlapping precast concrete blocks (1.5 m $\times$ 3 m $\times$ 0.16 m)

Fig. 7-3 - Earthfill embankment with a rockfill upstream protection and reinforced earth downstream slope construction : Jordan II, Gatton QLD (Australia, 1992) on 22 Feb. 1998 - H = 5.3 m, h = 1.4 m, $\alpha = 17.7^{o}$ - View from downstream

For an earth dam with overflow precast block stepped spillway, the most important criterion is the stability of the dam material. Seepage may occur in a saturated embankment and the resulting uplift pressures can damage or destroy the stepped channel and the dam : adequate drainage is essential. In a typical design, the blocks lay on a filter and erosion protection layer. The layer has the functions of filtering the seepage flow out of the subsoil and protecting the subsoil layer from erosion by flow in the drainage layer. The protection layer reduces or eliminates the uplift pressures acting on the concrete blocks. Usually a geotextile membrane is laid on the embankment before the placing of the layer, and another covers the protection layer before the installation of the blocks.

There is a basic design rule for precast concrete block systems : a skimming flow in a straight prismatic chute. The step block system was developed for a skimming flow regime : i.e., maximum block stability can only be achieved in skimming flows (e.g. BAKER 2000).

Alternatives for embankment stepped overflow

Alternative overtopping protection systems include timber cribs, sheet-piles, riprap and gabions, and reinforced earth. Timber crib overflows were used as early as the 18th century in Russia and some recent structures are still in use in Australia (CHANSON 2001). A number of weirs were designed with

steel sheet-piles and concrete slabs in Russia and Australia. An experimental structure was built with a reinforced-earth stepped overflow (Fig. 7-3). Another alternative is an overflow system made with gabions and Reno mattresses (e.g. CHANSON 1995a).

8. Hydraulic design of embankment overflow stepped spillways

8.1 Presentation

The design of embankment overflow stepped spillway is a critical issue. Any single failure of the spillway system can lead to a total dam failure. The professional community lacks basic design guidelines and current expertise is empirical.

For the design of an embankment overflow stepped spillway, a number of specific key issues must be assessed accurately and this includes :

[1] **Stepped spillway operation and chute erosion**

The stepped chute is designed to dissipate safely some kinetic energy, without damage to the steps. The spillway flow conditions cannot be calculated as for conventional flat (smooth invert) chutes.

[2] **Embankment seepage**

Seepage takes place in the embankment for high reservoir water levels. Strong interactions may occur between the free-surface flow and seepage flow in the embankment, that could cause uplift pressures leading to the destruction of the spillway, hence of the dam.

[3] **Drainage beneath steps**

A drainage system beneath the concrete steps is essential to prevent build-up of uplift pressures. Its purpose is to relieve pore pressure at the interface between the embankment and concrete steps. (Two stepped block spillways failed in Russia because of inadequate drainage layer (CHANSON 2000b).)

[4] **Sidewalls (overtopping, scour)**

The chute and crest sidewalls must be designed to prevent any overtopping for all flow rates up to PMF. The design of chute sidewalls must take into account the flow bulking resulting from the free-surface aeration. If splashing is acceptable, the training wall height may be sized to contain the characteristic air-water depth Y_{90} for all flow rates up to design flows. If the surroundings (e.g. embankment) are at risk of erosion, the sidewall height must be designed for $1.4*Y_{90}$. When the

developing spray can lead to fog or ice on surrounding roads or settlements, a greater safety margin must be considered. Note that the calculations of sidewall heights depend upon the type of flow regime (nappe, transition, skimming flow regimes).

Further strong secondary currents exist at the connection between the steps and the abutment walls. These are associated with high risks of scour, and the connections steps/abutment must be reinforced adequately.

[5] **Sidewalls (chute convergence effects)**

When the overflow spillway extends across the entire dam crest (e.g. Melton dam, Australia), the topography of the valley induces a convergence of the overflow. While a slight chute convergence may not affect the overall flow patterns, a reduction in channel width causes a modification of the discharge per unit width q_W and possibly a change in flow regime. Flow conditions at transition between flow regime could exhibit some instabilities leading to deflecting nappes and fluctuating hydrodynamic loads on the steps.

In nappe and skimming flows, sidewall convergence may further cause free-surface instabilities, including shock waves, flow concentrations, secondary currents and sidewall splashing that may be unacceptable.

[6] **Downstream energy dissipation and scour**

At the downstream end of the stepped chute, further energy dissipation takes place beneath the hydraulic jump or in the plunge pool for high tailwater levels. Turbulent fluctuations (velocity and pressure) in the hydraulic jump and at the plunge point may cause damage to the chute toe and sidewalls.

8.2 Discussion

Secondary currents at the connection between steps and (smooth) abutment walls

At the connection between the steps and the abutment walls ([8]), the differences in flow resistance between stepped invert and smooth concrete abutment generate transverse velocity gradient. Strong secondary currents associated with high shear forces develop and the risks of scour are high.

[8]This is especially important when the abutment is not a vertical concrete wall.

Major scour at abutments was observed during a number of flood events above overflow stepped weirs in Queensland : e.g., Whetstone weir (1953 overflow), Bonshaw weir (1956 failure) (CHANSON 2000b). In a keynote lecture on stepped block spillways, Dr BAKER emphasised that a known construction weakness is the joint between the chute invert and the sidewalls (BAKER 2000). (At Brushes Clough stepped spillway (UK), two longitudinal concrete guides were built to facilitate the installation of the blocks and the connection with the stone-pitched sidewalls.)

Chute convergence

To date, nearly all bibliography on stepped chute hydraulics applies to prismatic rectangular channels. Literature on converging stepped chutes is rare, but for TALBOT et al. (1997).

In nappe and skimming flows, sidewall convergence may cause shock waves propagating across the chute and impacting onto the opposite chute walls. At Gold Creek dam stepped spillway (Australia), significant flow disturbances and sidewall splashing caused by shock waves was observed during a 1996 overflow (CHANSON and WHITMORE 1998). Shock waves cause further flow concentrations and induce three-dimensional instabilities that may not be acceptable (CHANSON 2001, chap. 9).

Interactions between seepage and free-surface flows

During overflows, seepage takes place in the embankment. It is influenced by the infiltration into the downstream slope caused by the spillway flow, in addition to the flow through the embankment itself. Appropriate provision for drainage and evacuation of seepage flow through the steps is required. Drains are usually installed on the vertical face of the steps (Fig. 7-2, 8-1).

In skimming flows, the seepage that is drained into the step cavity may affect the cavity recirculation and in turn the turbulent dissipation process. It may lead to a reduction in flow resistance and an increase of the flow velocity at the downstream of the chute (i.e. at the plunge point, hydraulic jump or ski jump).

Flow resistance in skimming flows is a form drag mechanism predominantly (RAJARATNAM 1990, CHANSON et al. 2000). With form drag, fluid injection in the separated region (i.e. the cavity) does reduce drastically the drag (e.g. WOOD 1964, NAUDASCHER and ROCKWELL 1994). Table 8-1 summarises well-known studies, illustrated in Figure 8-2. A related case is the flow above a porous sill.

The writers hypothesise that a similar mechanism may exist in skimming flows above embankment stepped spillway. Note that this drag reduction mechanism differs and may add to drag reduction induced by free-surface aeration (see Paragraph 6.3).

Fig. 8-1 - Interactions between seepage flow and cavity recirculation

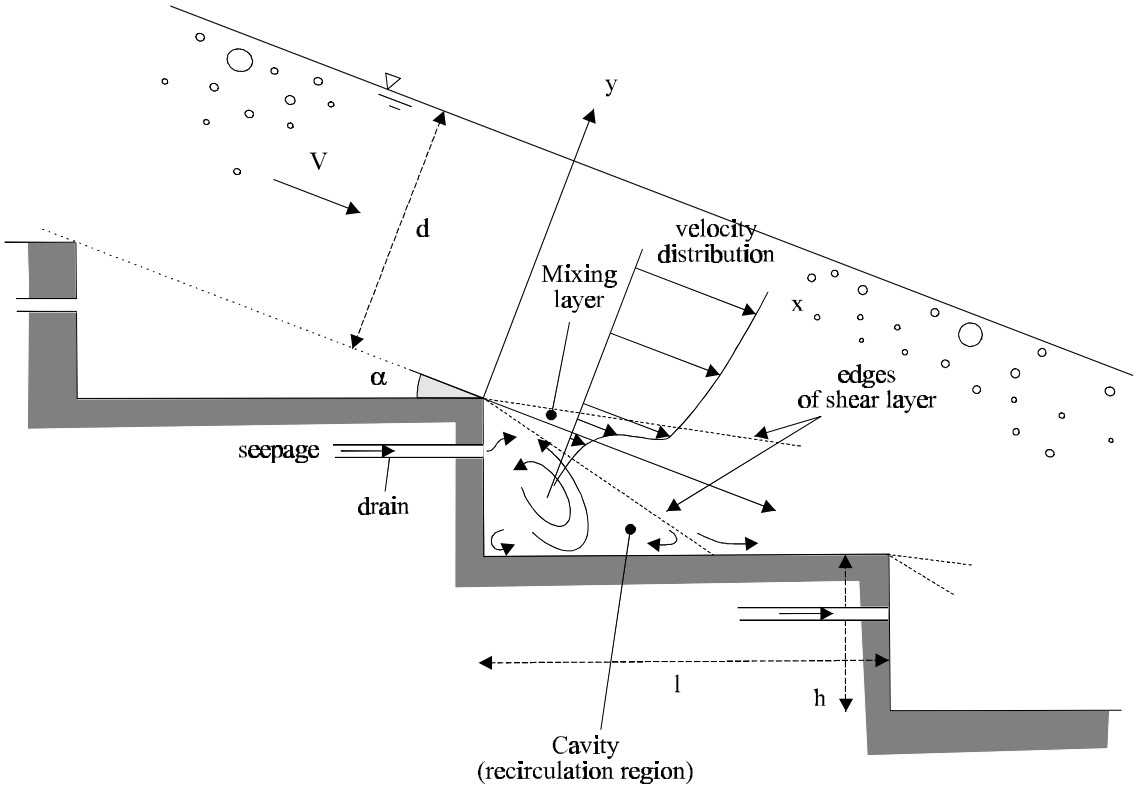

Figure 8-2 - Drag reduction behind bluff body associated with fluid injection
(A) Sketch of WOOD's (1964) experiments

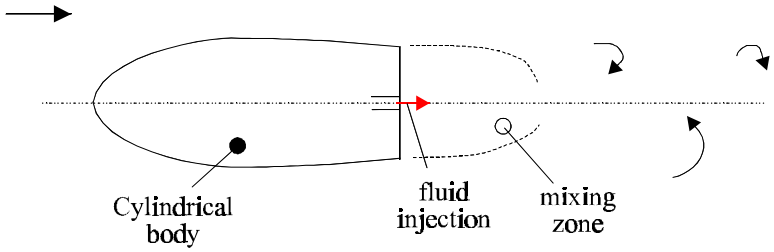

(B) Drag coefficient C_d on ventilated wings as a function of the dimensionless cavity length l_{cav}/h which is a function (VERRON and MICHEL 1984)

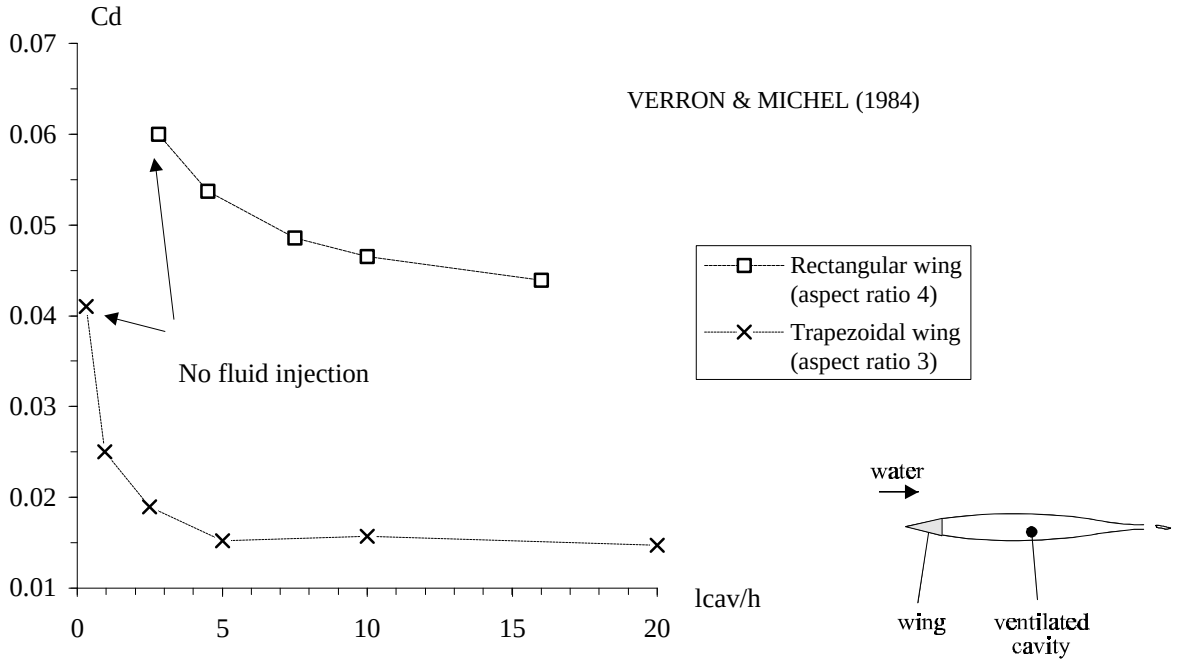

Downstream energy dissipation in a plunge pool

At the downstream end of the spillway, energy dissipation is usually achieved by (1) a high velocity water jet taking off from a flip bucket and impinging into a downstream plunge pool acting as a water cushion (e.g. Sosnovsky farm dam, Fig. 7-2), (2) a standard stilling basin downstream of the spillway where a hydraulic jump is created to dissipate a large amount of flow energy (e.g. U.S. Bureau of Reclamation designs), or (3) a plunge pool for high tailwater levels. In the latter case, the stability of the steps immediately beneath the plunge point (i.e. below tailwater level) is at risk (Fig. 8-3). Potential scour of the submerged steps is an issue that should be investigated in details with physical modelling.

BAKER (2000) observed major damage to stepped block spillway sections submerged by a hydraulic jump and a plunge pool. He illustrated his keynote lecture with an audio-visual documentary. YASUDA and OHTSU (2000) investigated the characteristics in the plunge pool downstream of a stepped chute as a function of the tailwater level. Although their results did not include efforts on the submerged steps, they observed some energy dissipation contribution from the submerged steps, suggesting some loads on the steps. The writers believe that this mode of failure is the worst for embankment overflow stepped spillways.

Table 8-1 - Drag reduction induced by fluid injection behind a bluff body

Reference (1)	Flow situations (2)	Description (3)
Fluid injection		
WOOD (1964)	Air flow past aerofoil with base bleed.	Drag reduction by fluid injection. Up to 60% drag reduction.
ABDUL-KHADER and RAI (1980)	Open channel flow past bridge piers ($0.2 < Fr < 0.65$).	Drag reduction with slotted piers. Up to 50% drag reduction.
SURYANARAYANA et al. (1993), SURYANARAYANA and PRABHU (2000)	Wind flow past a sphere.	Drag reduction by ventilation of the wake. Up to 60% drag reduction.
Cavity ventilation		
MICHEL and ROWE (1974)	Water flow past hydrofoil wings. Air ventilation.	Drag reduction with air ventilation at downstream end. Up to 83% drag reduction.
VERRON and MICHEL (1984)	Water flow past hydrofoil wings (rectangular and trapezoidal). Air ventilation	Drag reduction with air ventilation behind the wings. Up to 65% drag reduction.
Porous bluff body		
COOK (1990)	Wind flow past porous fences.	Drag reduction with increasing porosity : Drag $\propto (1 - C^2)$, C being the porosity.

Fig. 8-3 - Flow patterns at the plunge point

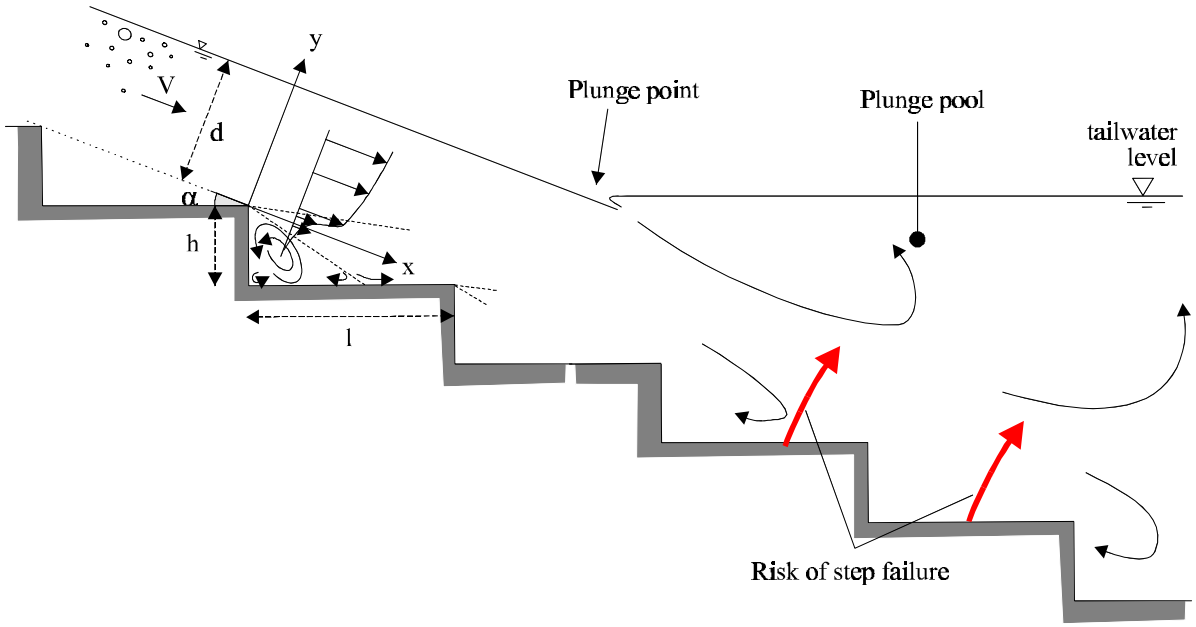

9. Conclusion

New experiments were conducted in a large-size stepped chute (1V:2.5H, h = 0.1 m, W = 1 m). Visual observations demonstrated three types of flow regimes : nappe flow, transition flow and skimming flow. The transition flow regime was observed for a relatively broad range of flow rates. It was characterised by a chaotic flow motion, strong splashing and very significant aeration.

Detailed air-water flow measurements were conducted in both transition and skimming flows immediately downstream of the inception point of free-surface aeration. In skimming flows, a complete characterisation was developed for the distributions of void fraction, bubble count rate and velocity. Although the air concentration distribution has the same shape as smooth chute flows, a slightly different trend was consistently observed, associated with strong droplet ejections. Flow resistance data are consistent with re-analysed data obtained in large-size laboratory chutes (Fig. 6-2). The re-analysis of all data highlights three dominant values of Darcy friction factor that are hypothesised to be three different modes of excitation. Drag reduction caused free-surface aeration was observed (Eq. (6-4), Fig. 6-5). It is believed to be caused by interactions between small entrained bubbles and developing mixing layers at each step edge.

Transition flows exhibited significantly different air-water flow properties from those observed in skimming flows. For each experiment, a deflected nappe was observed occasionally (i.e. at one step). The deflected jet was highly aerated and the associated spray would overtop the 1.25 m high sidewall.

Although the study was limited to one slope and for a short canal, the results highlighted the complexity of the free-surface aeration down stepped cascades.

For ancient embankments and new earthfill dams, an overflow stepped spillway may be considered as a main flood release structure. A number of design alternatives exists : concrete protection layer, precast concrete blocks, timber cribs, gabions. The hydraulic design of such stepped spillways includes a number of specific aspects which must be taken into account, including seepage beneath the steps, interactions between seepage and free-surface flows, and downstream energy dissipation in plunge pool for high tailwater levels. Step stability below the plunge point is probably the worst loading scenario for high tailwater levels and it must be investigated with a physical model in absence of experimental data.

It is believed that embankment overflow stepped spillways have a number of specific features that must be considered carefully, and that further experimental works is required to understand the interactions

between seepage and free-surface flows.

Acknowledgements

The writers thank Dr John MACINTOSH, Water Solutions, for his detailed review and comments. They acknowledge the assistance of M. EASTMAN, N. VAN SCHAGEN, and G. ILLIDGE (The University of Queensland). The first author thanks Professor APELT, Dr MATOS, Professor OHTSU, Dr ROYET, and Dr YASUDA for helpful discussions and for providing their experimental data.

Appendix I - Summary of experimental results

Tableau I-1 - Single-tip conductivity probe data (Series 1)

Q_w m^3/s	Location	$\frac{Y_{90}}{d_c}$	C_{mean}	$\frac{(F_{ab})_{max} * d_c}{V_c}$	$\frac{U_w}{V_c}$
(1)	(2)	(3)	(4)	(5)	(6)
Series 1					
0.1819	Step edge 6	0.44	0.15	4.30	2.64
0.1819	Step edge 7	0.52	0.24	7.59	2.55
0.1819	Step edge 8	0.51	0.28	13.38	2.71
0.164	Step edge 6	0.45	0.16	5.24	2.64
0.164	Step edge 7	0.55	0.31	9.79	2.62
0.164	Step edge 8	0.53	0.29	15.45	2.66
0.1467	Step edge 5	0.44	0.13	3.50	2.60
0.1467	Step edge 6	0.49	0.24	8.68	2.69
0.1467	Step edge 7	0.59	0.36	12.96	2.63
0.1467	Step edge 8	0.59	0.34	16.98	2.56
0.1301	Step edge 5	0.44	0.15	3.52	2.68
0.1301	Step edge 6	0.52	0.27	9.48	2.64
0.1301	Step edge 7	0.65	0.42	15.37	2.65
0.1301	Step edge 8	0.60	0.35	18.39	2.56
0.1237	Step edge 5	0.46	0.19	5.30	2.71
0.1237	Step edge 6	0.54	0.32	13.21	2.74
0.1237	Step edge 7	0.69	0.41	15.91	2.48
0.1237	Step edge 8	0.61	0.36	18.57	2.58
0.1142	Step edge 5	0.46	0.22	5.16	2.76
0.1142	Step edge 6	0.56	0.36	13.07	2.79
0.1142	Step edge 7	0.76	0.43	16.37	2.31
0.1142	Step edge 8	0.63	0.36	19.43	2.47
0.103	Step edge 4	0.44	0.14	2.85	2.67
0.103	Step edge 5	0.54	0.28	7.34	2.56
0.103	Step edge 6	0.68	0.46	14.33	2.70
0.103	Step edge 7	0.76	0.48	15.29	2.51
0.103	Step edge 8	0.57	0.34	18.63	2.65
0.099	Step edge 4	0.43	0.13	2.87	2.64
0.099	Step edge 5	0.56	0.33	8.52	2.66
0.099	Step edge 6	0.75	0.52	13.77	2.77
0.099	Step edge 7	0.63	0.35	16.97	2.46
0.099	Step edge 8	0.62	0.43	18.69	2.80
0.0845	Step edge 4	0.49	0.22	4.05	2.63
0.0845	Step edge 5	0.76	0.53	10.04	2.81
0.0845	Step edge 6	0.64	0.44	14.49	2.79
0.0845	Step edge 7	0.69	0.46	15.10	2.68
0.0845	Step edge 8	0.62	0.43	17.68	2.83
0.0799	Step edge 4	0.55	0.30	4.59	2.60
0.0799	Step edge 5	0.85	0.56	10.14	2.65
0.0799	Step edge 6	0.67	0.39	13.61	2.45
0.0799	Step edge 7	0.73	0.44	15.42	2.44
0.0799	Step edge 8	0.65	0.40	16.99	2.53
0.0708	Step edge 3	0.43	0.13	1.79	2.68
0.0708	Step edge 4	0.55	0.38	5.67	2.92
0.0708	Step edge 5	0.62	0.40	10.82	2.69
0.0708	Step edge 6	1.07 (*)	0.68 (*)	11.31	2.94
0.0708	Step edge 7	0.68	0.43	14.43	2.58
0.0708	Step edge 8	0.89	0.57	15.46	2.59

0.0665	Step edge 3	0.44	0.15	1.81	2.63
0.0665	Step edge 4	0.66	0.48	4.65	2.89
0.0665	Step edge 5	0.69	0.43	10.19	2.55
0.0665	Step edge 6	1.47 (*)	0.73 (*)	10.26	2.52
0.0665	Step edge 7	0.82	0.48	13.45	2.35
0.0665	Step edge 8	0.85	0.50	14.89	2.37
0.0643	Step edge 3	0.46	0.18	1.97	2.65
0.0643	Step edge 4	0.75	0.52	4.47	2.79
0.0643	Step edge 5	0.74	0.49	9.37	2.65
0.0643	Step edge 6	1.55 (*)	0.77 (*)	9.92	2.79
0.0643	Step edge 7	0.85	0.54	12.51	2.55
0.0643	Step edge 8	0.67	0.44	14.44	2.69
0.058	Step edge 3	0.51	0.24	2.22	2.58
0.058	Step edge 4	0.88	0.60	5.62	2.86
0.058	Step edge 5	0.82	0.52	9.00	2.55
0.058	Step edge 6	1.62 (*)	0.78 (*)	9.81	2.79
0.058	Step edge 7	0.81	0.51	12.06	2.48
0.058	Step edge 8	0.73	0.48	13.51	2.62
0.0519	Step edge 3	0.62	0.38	3.53	2.62
0.0519	Step edge 4	1.08	0.64	6.33	2.58
0.0519	Step edge 5	0.77	0.49	8.88	2.55
0.0519	Step edge 6	1.21 (*)	0.74 (*)	8.49	3.14
0.0519	Step edge 7	0.81	0.49	11.18	2.43
0.0519	Step edge 8	1.00 (*)	0.65 (*)	11.77	2.83
0.046	Step edge 3	0.56	0.36	3.24	2.78
0.046	Step edge 4	0.89	0.59	6.97	2.72
0.046	Step edge 5	0.72	0.48	9.22	2.65
0.046	Step edge 6	1.05 (*)	0.63 (*)	9.06	2.61
0.046	Step edge 7	0.72	0.48	10.14	2.65
0.046	Step edge 8	1.14 (*)	0.68 (*)	9.63	2.77

Notes : Column (2) : the first step edge is located at the downstream end of the broad-crest; $U_W = q_W/d$; (*) deflected nappe.

Tableau I-2 - Double-tip conductivity data (Series 2)

Q_W m^3/s	Location	$\frac{Y_{90}}{d_C}$	C_{mean}	$\frac{(F_{ab})_{max} * d_C}{V_C}$	$\frac{U_W}{V_C}$	$\frac{V_{90}}{V_C}$	$a_{mean} * d_C$
(1)	(2)	(3)	(4)	(5)	(6)	(7)	(8)
Series 2							
0.1819	Step edge 6	0.51	0.23	7.70	2.55	2.63	3.6
0.1819	between step edges 6 & 7	0.50	0.31	9.92	2.89	2.73	8.1
0.1819	Step edge 7	0.47	0.23	13.60	2.77	2.79	9.1
0.1819	between step edges 7 et 8	0.60	0.40	15.19	2.77	2.73	16.4
0.1819	Step edge 8	0.59	0.38	16.37	2.75	2.85	15.7
0.1142	Step edge 5	0.45	0.26	11.20	2.98	2.84	6.6
0.1142	Step edge 6	0.65	0.50	18.55	3.05	2.86	16.3
0.1142	Step edge 7	0.59	0.43	27.38	2.96	3.00	24.7
0.1142	between step edges 7 et 8	0.64	0.53	21.68	3.32	2.88	26.1
0.1142	Step edge 8	0.54	0.43	29.94	3.23	2.99	29.2
0.058	Step edge 3	0.46	0.20	4.06	2.73	2.65	1.5
0.058	Step edge 4	0.85	0.63	10.43	3.17	2.74	6.7
0.058	Step edge 5	0.78	0.56	13.74	2.91	2.30	13.9
0.058	Step edge 6	1.24 (*)	0.76 (*)	16.45	3.40	2.75	12.1
0.058	Step edge 7	0.79	0.55	19.64	2.86	3.48	17.3

0.058	Step edge 8	0.66	0.52	21.13	3.19	3.09	21.7

Notes : Column (2) : the first step edge is located at the downstream end of the broad-crest; $U_W = q_W/d$; (*) deflected nappe; a_{mean} : depth-averaged specific interface area.

Appendix II - Modelling cavity ejection processes (by H. CHANSON)

In skimming flows, recirculating vortices develop in the step cavities and they are maintained through the transmission of shear stress from the mainstream and by unsteady momentum exchanges between the main stream and cavity flows. At irregular time intervals, some cavity volume flows outwards and is replaced by fresh fluid (Fig. 3-3). The duration of the cavity ejection (or burst) is relatively short compared to the average ejection period. The ejections and inflows occur predominantly in the downstream region of the cavity ([9]). Several researchers suggested that the initiating mechanisms of the ejections resides within the fully-developed flow and not in the cavity flow itself, the ejection process being caused by interactions between low-speed streaks and vorticity structures next to the pseudo-bottom formed by the step edges (DJENEDI et al. 1994, ELAVARASAN et al. 1995).

An early cavity ejection model

ETHEMBABAOGLU (1978) developed a model of hydrodynamic instability in the free-shear layer. Vortices form in the shear layer. They are convected downstream, interacting with the downstream edge of the cavity and inducing disturbances which are in turn transmitted to the origin of the shear layer. The process generate self-induced disturbances.

The frequency of instability ([10]) may be estimated analytically. For a triangular cavity, it yields :

$$\frac{F_{ej} * (h*\cos\alpha)}{V} = 0.5 * \left(i + \frac{1}{4}\right) * \sin\alpha * \cos\alpha \qquad \text{(II-1)}$$

where V is the mainstream velocity, $h*\cos\alpha$ is the cavity depth, and i is an integer. For ratios of cavity length to cavity depth L_{cav}/k_S less than 2, Equation (II-1) was close to ETHEMBABAOGLU's observations using i = 1 and 2. For greater cavity length ratios, i = 2 and 3 gave better agreement.

---

[9]Stepped chute data : Present study. Strip roughness data : DJENEDI et al. (1994), ELAVARASAN et al. (1995).

[10]which is basically the frequency of fluid ejections.

Energy considerations

Considering a skimming flow, it is hypothesised that all the energy losses occur by viscous dissipation in the cavity, with some energy exchange between the main flow and the recirculation by irregular fluid ejections. Considering the flow region located between two adjacent step edges (Fig. II-1), and during an average ejection period ΔT ([11]), the continuity equation for the cavity implies :

$$Q_{out} * \Delta t = Q_{in} * \Delta t = \forall_{ej} \qquad \text{(II-2a)}$$

where Q_{in} and Q_{out} are the inflow and outflow rates respectively, $\forall_{ej}$ is the volume of ejected fluid, Δt is the ejection ([12]) duration. Dividing by the ejection period ΔT, Equation (II-2) may be rewritten :

$$Q_{out} * \frac{\Delta t}{\Delta T} = \forall_{ej} * F_{ej} \qquad \text{(II-2b)}$$

where $F_{ej} = 1/\Delta T$ is the fluid ejection frequency.

At uniform equilibrium, the rate of energy loss between two adjacent step edges equals $\rho*Q*h$, where ρ is the fluid density, Q is the flow rate and h is the vertical step height. The energy is dissipated in the recirculation cavity at a rate $\rho*\forall_{ej}*F_{ej}*\Delta T/\Delta t*(V^2/(2*g) - V_{out}^2/(2*g))$, where V_{out} is the outflow velocity, and the inflow velocity is assumed to be equal to the flow velocity V. The energy principle yields a relationship between the dimensionless fluid ejection frequency and rate of energy loss:

$$\frac{F_{ej} * (h*\cos\alpha)}{V} = \frac{2 * W * h^2 * \cos\alpha * \frac{\Delta t}{\Delta T}}{\forall_{ej} * \frac{V^2}{g*d} * \left(1 - \frac{V_{out}^2}{V^2}\right)} \qquad \text{(II-3a)}$$

where W is the chute width. For a wide channel with flat horizontal steps, it becomes :

$$\frac{F_{ej} * (h*\cos\alpha)}{V} = \frac{f * \frac{\Delta t}{\Delta T}}{2 * \lambda * \left(1 - \frac{V_{out}^2}{V^2}\right)} \qquad \text{Flat horizontal steps (II-3b)}$$

where f is the dimensionless pseudo-bed shear stress, or Darcy friction factor, and λ is the ratio of the

---

[11]The calculations are developed for an incompressible flow. Note that $\Delta T = 1/F_{ej}$ where F_{ej} is the fluid ejection frequency.

[12]A fluid ejection is sometimes called a burst or bursting event.

average fluid ejection volume V_{ej} to the total cavity volume.

Discussion

A lower limit of the average ejection frequency is set for $V_{out}/V << 1$ and by assuming that the ejection volume equals the cavity volume. For flat horizontal steps, it yields :

$$\left(\frac{F_{ej} * (h*\cos\alpha)}{V}\right)_{min} = \frac{f}{2} * \frac{\Delta t}{\Delta T} \qquad \text{Flat horizontal steps (II-4)}$$

The duration of fluid ejection Δt must be less than the average ejection period ΔT. Combining with the continuity equation for the cavity, it yields an upper limit of the average ejection frequency :

$$\left(\frac{F_{ej} * (h*\cos\alpha)}{V}\right)_{max} = \frac{\frac{\Delta t}{\Delta T}}{\lambda * \left(1 + \frac{V}{V_{out}}\right)} \qquad \text{Flat horizontal steps (II-5)}$$

Equations (II-3), (II-4) and (II-5) are shown in Figure II-2. Calculations were performed for f = 0.2, λ = 0.5, and $\Delta T/\Delta t$ = 7. (Flow visualisations in stepped chute models (e.g. Present study) suggest a typical value of λ = 0.5 while visualisations of d-type cavity flows showed a ratio of average ejection period to ejection duration of about 5.5 to 8 (Table II-1).) Assuming that all energy losses take place by viscous dissipation in the recirculation cavity, the analytical solution must satisfy :

$$\left(\frac{F_{ej} * (h*\cos\alpha)}{V}\right)_{min} \leq \frac{F_{ej} * (h*\cos\alpha)}{V} \leq \left(\frac{F_{ej} * (h*\cos\alpha)}{V}\right)_{max} \qquad \text{(II-6)}$$

Using Equations (II-3), (II-4) and (II-5), it yields that the ratio of outflow velocity to inflow velocity is centered around 0.5 :

$$\frac{1}{2} * \left(1 - \sqrt{1 - f}\right) < \frac{V_{out}}{V} < \frac{1}{2} * \left(1 + \sqrt{1 - f}\right) \qquad \text{(II-7)}$$

A further conditions is $f \leq 1$.

Fig. II-1 - Sketch of a cavity ejection

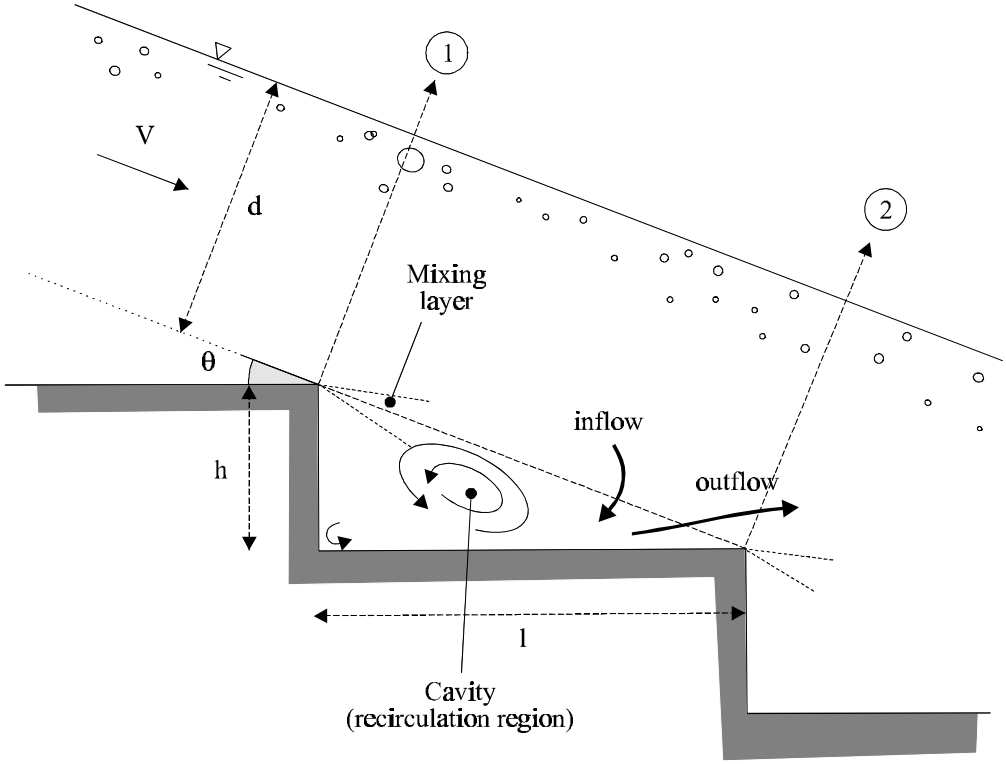

Fig. II-2 - Dimensionless average ejection frequency

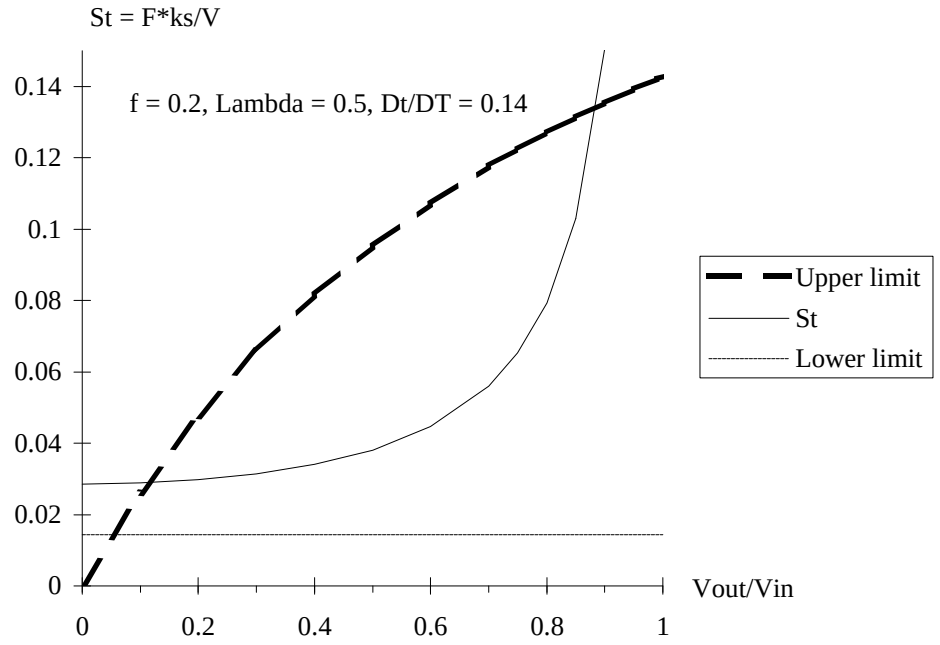

Table II-1 - Experimental observations of cavity ejections

Reference	Average ejection frequency $\frac{F_{ej} * k_s}{V_o}$	Ejection duration $\frac{k_s}{V_o * \Delta t}$	Comments
(1)	(2)	(3)	(4)
Fully-developed flows			
HEIDRICK et al. (1977)	$1.25E\text{-}3 * f * \frac{V_o * k_s}{\nu}$	--	Smooth pipe water flows ($\varnothing$ = 0.0787 m). Fully-developed flows. V_o = 0.4 to 2.6 m/s.
Boundary layer flows			
TOWNES and SABERSKY (1966)	$0.062 * \frac{k_s * V_o}{\nu} *$	--	Water tunnel (W = 0.851 m). V_o = 0.04 to 0.25 m/s. Square cavities : k_s = 0.0032 to 0.0254 m.
ETHEMBABAOGLU (1978)	0.3 to 0.58	--	Water tunnel (d = 0.1 m, W = 0.24 m). V_o = 5.5 to 7.5 m/s, δ_{BL} = 0.036 m, δ_* = 0.0042 m. Single rectangular cavities : k_s = 0.1 m, L_{cav}/k_s = 1.9 to 3.6.
BANDYOPDHAY (1987)	$\sim 1.2 * \frac{k_s * V_o}{\nu}$	--	Wind tunnel (d = 0.18 m, W = 0.28 m). V_o < 40 m/s. Rectangular cavities : k_s = 0.003 m, L_{cav}/k_s = 0.7 to 3.0.
DJENEDI et al. (1994)	$0.182 * \frac{k_s}{\delta_{BL}}$	$\frac{k_s}{\delta_{BL}}$	Water tunnel (d = 0.26 m, W = 0.26 m). V_o = 0.4 m/s, δ_{BL} = 0.035 m, δ_M = 0.0025 m. Square cavities : k_s = 5 mm.
TANTIRIDGE et al. (1994)	0.017	0.138	Square tunnel (d = 0.025 m, W = 0.025 m). Fully-developed inflow. V_o = 0.43 m/s. Triangular cavity : k_s = 1.5 mm, α = 45°.
Open channel flows			
SUMER et al. (2001)	0.05	0.3	Open channel flow (d = 0.4 m, V ~ 0.4 m/s) over large stones (k_s = 0.0385 m).

Notes : d : channel height or flow depth; F_{ej} : average ejection frequency; k_s : cavity depth (or roughness height); L_{cav} : cavity length; V_o : free-stream velocity; δ_{BL} : boundary layer thickness; δ_* : displacement thickness; δ_M : momentum thickness; Δt : ejection (burst) duration.

Appendix III - Air bubble diffusion in self-aerated flows (by H. CHANSON)

In supercritical flows, free-surface aeration is often observed. The phenomenon, called 'white waters', occurs when turbulence acting next to the free-surface is large enough to overcome both surface tension for the entrainment of air bubbles and buoyancy to carry downwards the bubbles. Assuming a homogeneous air-water mixture for C < 90%, the advective diffusion of air bubbles may be analytically predicted. At uniform equilibrium, the air concentration distribution is a constant with respect to the distance x in the flow direction. The continuity equation for air in the air-water flow yields :

$$\frac{\partial}{\partial y}\left(D_t * \frac{\partial C}{\partial y}\right) = \cos\alpha * \frac{\partial}{\partial y}(u_r * C) \quad \text{(III-1)}$$

where D_t is the turbulent diffusivity, u_r is the bubble rise velocity, α is the channel slope and y is measured perpendicular to the mean flow direction. Tche bubble rise velocity in a fluid of density ρ_w*(1-C) equals :

$$u_r^2 = [(u_r)_{Hyd}]^2 * (1 - C) \quad \text{(III-2)}$$

where $(u_r)_{Hyd}$ is the rise velocity in hydrostatic pressure gradient (CHANSON 1995b,1997b). A first integration of the continuity equation for air in the equilibrium flow region leads to :

$$\frac{\partial C}{\partial y'} = \frac{1}{D'} * C * \sqrt{1 - C} \quad \text{(III-3)}$$

where $y' = y/Y_{90}$ and $D' = D_t/(u_r)_{Hyd}*\cos\alpha*Y_{90})$ is a dimensionless turbulent diffusivity. D' is the ratio of the air bubble diffusion coefficient to the rise velocity component normal to the flow direction times the characteristic transverse dimension of the shear flow.

Assuming a homogeneous turbulence across the flow (i.e. D' constant), it yields :

$$C = 1 - \tanh^2\left(K' - \frac{y'}{2 * D'}\right) \quad \text{(III-4)}$$

where tanh is the hyperbolic tangent function and K' a dimensionless integration constant (CHANSON 1995b,1997b). A relationship between D' and K' is deduced for C = 0.9 for y' = 1 :

$$K' = K^* + \frac{1}{2 * D'} \quad \text{(III-5)}$$

where $K^* = \tanh^{-1}(\sqrt{0.1}) = 0.32745015...$ The diffusivity and the mean air content C_{mean} defined in terms of Y_{90} are related by :

$$C_{mean} = 2 * D' * \left(\tanh\left(K^* + \frac{1}{2 * D'}\right) - \tanh(K^*)\right) \quad \text{(III-6)}$$

Advanced void fraction distribution models may be developed assuming a non constant diffusivity. Results are shown in Table III-1. Columns (1) and (2) show the analytical solutions of the air concentration and air bubble diffusivity distributions respectively. Column (3) lists successful applications of the solution, the reference data being listed below.

Table III-1 - Analytical solutions of Equation (III-3)

C (1)	D' (2)	Domain of applications (3)	Remarks (4)
$0.9 * \sqrt{\frac{y}{Y_{90}}}$	$\frac{2}{0.9^2} * C^2 * \sqrt{1 - C}$	Transition flow ([a])	$C_{mean} = 0.60$.
$K''' * \left(1 - \exp\left(-\lambda * \frac{y}{Y_{90}}\right)\right)$	$\frac{C * \sqrt{1 - C}}{\lambda * (K''' - C)}$	Transition flow ([a])	$K''' = \frac{0.9}{1 - \exp(-\lambda)}$ $C_{mean} = K''' - \frac{0.9}{\lambda}$ Note : $C_{mean} > 0.45$
$1 - \tanh^2\left(K' - \frac{y/Y_{90}}{2 * D'}\right)$	Constant	Self-aerated flow, skimming flow ([a])	CHANSON (1995b,1997b) $K' = K^* + \frac{1}{2 * D'}$ $K^* = \tanh^{-1}(\sqrt{0.1}) = 0.32745015...$ $C_{mean} = 2 * D' * \left(\tanh\left(K^* + \frac{1}{2 * D'}\right) - \tanh(K^*)\right)$
$1 - \tanh^2\left(K' - \frac{(y/Y_{90})^2}{4 * \lambda}\right)$	$\frac{\lambda}{y/Y_{90}}$	Self-aerated flow	$K' = K^* + \frac{1}{4 * \lambda}$ $K^* = \tanh^{-1}(\sqrt{0.1}) = 0.32745015...$ $C_{mean} = \frac{1.7637E\text{-}3 + 0.8643*\lambda^{1.69}}{0.09547 + \lambda^{1.69}}$
$1 - \tanh^2\left(K' - \frac{(y/Y_{90})^{n+1}}{2 * (n + 1) * \lambda}\right)$	$\frac{\lambda}{(y/Y_{90})^n}$	Self-aerated flow	$K' = K^* + \frac{1}{2 * (n+1) * \lambda}$ $K^* = \tanh^{-1}(\sqrt{0.1}) = 0.32745015...$
$1 - \tanh^2\left(K' - \frac{y/Y_{90}}{2 * D_o} + \frac{\left(\frac{y}{Y_{90}} - \frac{1}{3}\right)^3}{3 * D_o}\right)$	$\frac{D_o}{1 - 2*\left(\frac{y}{Y_{90}} - \frac{1}{3}\right)^2}$	Skimming flow ([a])	$K' = K^* + \frac{1}{2 * D_o} - \frac{8}{81 * D_o}$ $K^* = \tanh^{-1}(\sqrt{0.1}) = 0.32745015...$ $C_{mean} = 0.7622*(1.0434 - \exp(-3.614*D_o))$

Note : ([a]) measured at step edges.
REFERENCE DATA : (1) Smooth-invert prototype: CAIN (1978). (2) Smooth invert laboratory: STRAUB and ANDERSON (1956), XI (1988). (3) Skimming flow (laboratory): RUFF and FRIZELL (1984), TOZZI et al. (1998), Present study. (4) Transition flow (laboratory): Present study.

Appendix IV - Velocity measurements and cross-correlation techniques for dual-tip probe measurements in gas-liquid flows

In turbulent gas-liquid flows, a velocity measurement technique is based upon the successive detection

of bubbles/droplets by two sensors : i.e., double tip optical and resistivity probes (Fig. IV-1). The technique assumes that {1} the probe sensors are aligned along a streamline, {2} the bubble/droplet characteristics are little affected by the leading tip, and {3} the bubble/impact impact on the trailing tip is similar to that on the leading tip. In highly turbulent gas-liquid flows, the successive detection of a bubble by each probe sensor is highly improbable, and it is common to use a cross-correlation technique (e.g. CROWE et al. 1998, pp. 309-318). The time-averaged air-water velocity is defined as:

$$V = \frac{\Delta x}{T} \qquad \text{(IV-1)}$$

where Δx is the distance between probe sensors and T is the travel time for which the cross-correlation function is maximum : i.e., $R(T) = R_{max}$ where R is the normalised cross-correlation function and R_{max} is the maximum cross-correlation value (Fig. IV-1).

The shape of the cross-correlation function provides a further information on the turbulent velocity fluctuations (Fig. IV-2). Flat cross-correlation functions are associated with large velocity fluctuations around the mean and large turbulence intensity Tu = u'/V, where u' is the standard deviation of the turbulent velocity fluctuations. Thin high cross-correlation curves are characteristics of small turbulent velocity fluctuations. The information must be corrected to account for the intrinsic noise of the leading probe signal and the turbulence intensity is related to the broadening of the cross-correlation function compared to the autocorrelation function (Fig. IV-1).

The definition of the standard deviation of the velocity leads to :

$$u'^2 = \frac{V^2}{N} \sum_{i=1}^{N} \frac{1}{t^2} * (t - T)^2 \qquad \text{(IV-2)}$$

where V is the mean velocity, N is the number of samples and t is the bubble travel time data. With an infinitely large number of data points N, an extension of the mean value theorem for definite integrals may be used as the functions $1/t^2$ and $(t-T)^2$ are positive and continuous over the interval [i = 1, N] (SPIEGEL 1974). It implies that there exists at least one characteristic bubble travel time t' satisfying $t_1 \leq t' \leq t_N$ such that :

$$\left(\frac{u'}{V}\right)^2 = \frac{1}{N} * \frac{1}{t'^2} * \sum_{i=1}^{N} (t - T)^2 \qquad \text{(IV-3)}$$

That is, the standard deviation of the velocity is proportional to the standard deviation of the bubble

travel time:

$$\frac{u'}{V} = \frac{\sigma_t}{t'} \qquad \text{(IV-4)}$$

Assuming that the successive detections of bubbles by the probe sensors is a true random process ([13]), the cross-correlation function would be a Gaussian distribution :

$$R(t) = R_{max} * \exp\left(- \left(\frac{t - T}{\sigma_T} \right)^2 \right) \qquad \text{(IV-5)}$$

where σ_T is the standard deviation of the cross-correlation function. Defining ΔT as a time scale satisfying : $R(T+\Delta T) = R_{max}/2$, the standard deviation equals : $\sigma_T = \Delta T/1.175$ for a true Gaussian distribution. The standard deviation of the bubble travel time σ_t is a function of both the standard deviations of the cross-correlation and autocorrelation functions :

$$\sigma_t = \frac{\sqrt{\Delta T^2 - \Delta t^2}}{1.175} \qquad \text{(IV-6)}$$

where Δt is the characteristic time for which the normalised autocorrelation function equals 0.5. Assuming that t' ~ T and that the bubble/droplet travel distance is a constant Δx, Equation (IV-4) implies that the turbulence intensity u'/V equals :

$$Tu = \frac{u'}{V} \approx 0.851 * \frac{\sqrt{\Delta T^2 - \Delta t^2}}{T} = Tu' \qquad \text{(IV-7)}$$

Tu' is a dimensionless velocity scale that is characteristic of the turbulent velocity fluctuations over the distance Δx separating the probe sensors. Although Tu' is not strictly equal to the dimensionless turbulent velocity fluctuation Tu = u'/V, the distributions of modified turbulence intensity Tu' provide some qualitative information on the turbulent velocity field in gas-liquid flows.

KIPPHAN (1977) developed a slightly different reasoning for two-phase mixtures such as pneumatic conveying. He obtained a result of similar form :

$$\frac{u'}{U_w} = \sqrt{\frac{\sigma_T^2 - \sigma'^2_t}{T^2}} \qquad \text{(IV-8)}$$

where U_w is the mean flow velocity, T is the mean particle travel time (e.g. on the conveyor, in the pipe) and σ'_t is the standard deviation of the autocorrelation function. It is believed however that

---

[13]For example, affected only by random advective dispersion of the bubbles and random velocity fluctuations over the distance separating the probe sensors.

KIPPHAN's result (Eq. (IV-8)) is an approximation ([14]).

Discussion

Equation (IV-7) has a wider range of application than Equation (IV-8) because it is applicable to turbulent shear flows (e.g. boundary layer flow). The modified turbulence intensity Tu' (Eq. (IV-7)) may provide both qualitative and quantitative information on the turbulent velocity field in gas-liquid flows.

The first writer's experience suggests that the standard deviation of the bubble travel time is also a function of the distance Δx between sensors. For a given bubbly flow configuration and probe sensors, the cross-correlation function broaden and the maximum cross-correlation decreases with increasing distance Δx. KIPPHAN (1977) recommended an optimum distance Δx between sensor equal to :

$$\frac{(\Delta x)_{opt}}{\delta x} \approx \frac{0.35}{Tu} \qquad \text{(IV-9)}$$

where δx is the characteristic sensor size in the flow direction. Equation (IV-9) does not account however for the characteristic size of the two-phase flow structure. Table IV-1 summarises successful designs of dual-tip resistivity probes. For these designs, the "optimum" probe spacing satisfies :

$$\frac{(\Delta x)_{opt}}{\delta x} = 33.5 * V_{max}^{0.27} \qquad \text{(IV-10)}$$

where V_{max} is the maximum bubbly flow velocity in m/s.

The result is further affected by an offset between the leading and trailing tips of the probe. For example, CHANSON (1995c,1997b) introduced successfully such an offset to reduce the effects of separation and wake downstream of the leading tip, reported by SENE (1984) and CHANSON (1988).

[14]The assumptions of t' ~ T and Equation (IV-7) are not strictly correct.

Table IV-1 - Characteristic dimensions of successful dual-tip resistivity probe designs

Reference	Δx m	δx m	$\Delta x/\delta x$	V m/s	Remarques
(1)	(2)	(3)	(4)	(5)	(6)
Resistivity probes					
SERIZAWA et al. (1975)	0.005	2.0E-4	25	0.5 to	Bubbly pipe flows.
CAIN (1978)	0.1016	2.0E-3	50.8	15.6 to 18.5	Prototype spillway flows (Aviemore, NZ).
LEWIS and DAVIDSON (1983)	0.0015	5.0E-4	3	0.17 to 0.68	Bubble column flows.
CHANSON (1988)	0.01	3.0E-4	33.3	7 to 17	Laboratory spillway flows
BEHNIA and GILLESPIE (1991)	0.00531	5E-4	10.6	up to 6	Bubbly pipe flows.
REVANKAR and ISHII (1992)	0.004	1.2E-4	33.3	0.1 to 1	Bubbly pipe flows.
LIU and BANKOFF (1993)	0.005	1.0E-4	50	0.4 to 1.4	Bubbly pipe flows.
CHANSON (1995c,1997b)	0.008	5.0E-5	160	1 to 9	Laboratory experiments : open channel flows, stepped cascade flows, plunging jet flows, water jets discharging into air.
Fibre optic probes					
CHABOT et al. (1992)	0.004 to 0.009	1E-3	4 to 9	0.5	Bubble column flows.

Fig. IV-1 - Sketch of a cross-correlation function and dual-tip probe

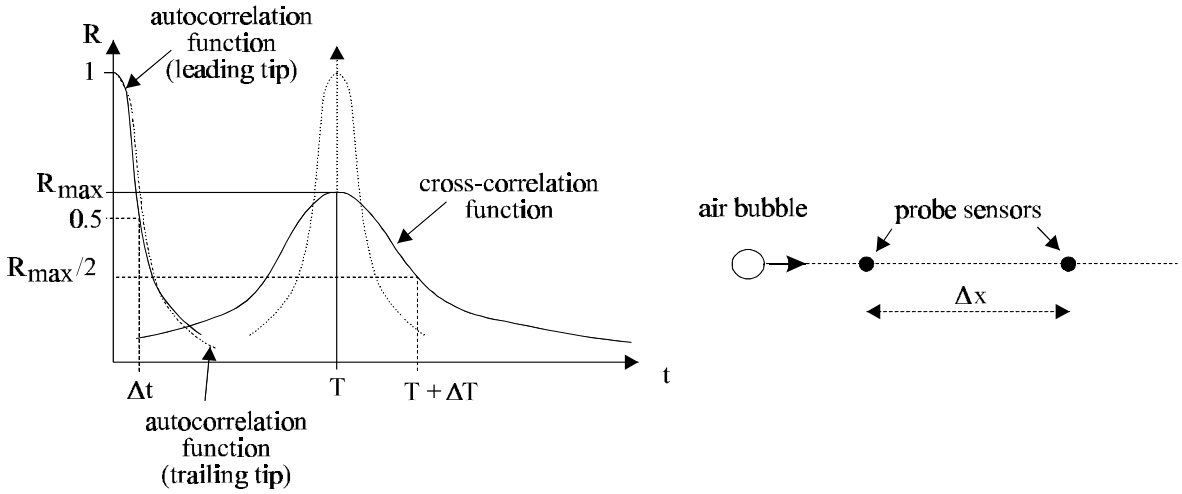

Fig. IV-2 - Examples of autocorrelation and cross-correlation functions (Run Q23)

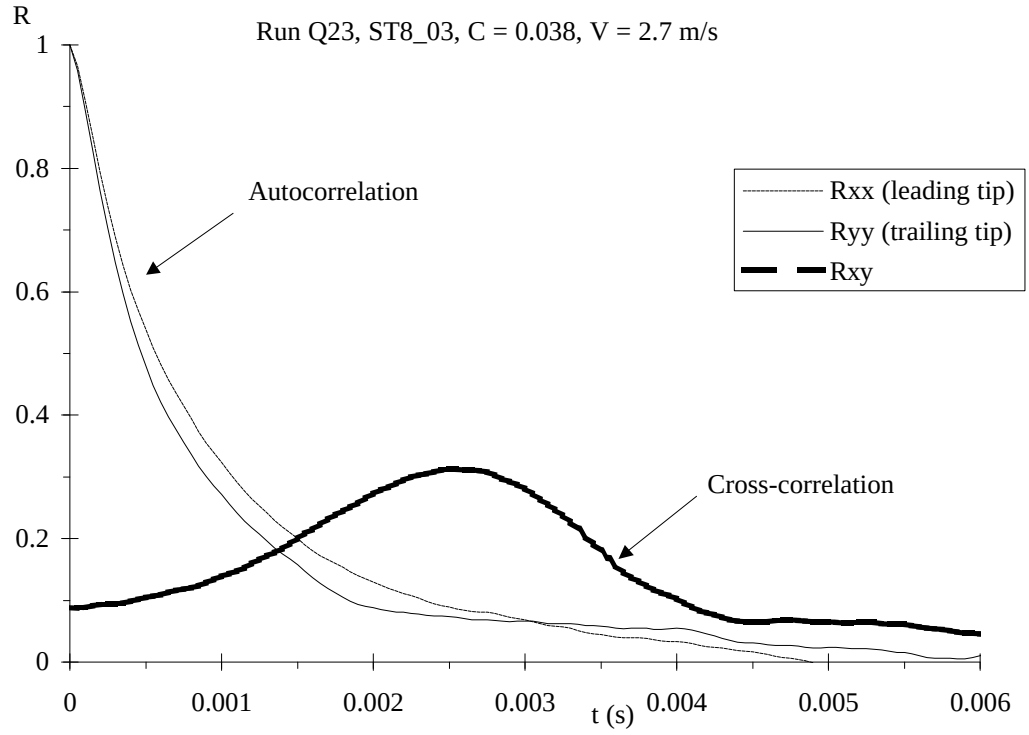

References

ABDUL-KHADER, M.H., and RAI, S.P. (1980). "A Study of Channel obstructions with a Longitudinal Slot." *Proc. 7th Australasian Hydraulics and Fluid Mechanics Conf.*, IEAust., Brisbane, Australia, pp. 175-178.

ACKERS, P., WHITE, W.R., PERKINS, J.A., and HARRISON, A.J.M. (1978). "Weirs and Flumes for Flow Measurement." *John Wiley*, Chichester, UK, 327 pages.

ANWAR, H.O. (1994). "Self-Aerated Flows on Chutes and Spillways - Discussion." *Jl of Hyd. Engrg.*, ASCE, Vol. 120, No. 6, pp. 778-779.

AZAIEZ, J. (2000). "Reduction of Free Shear Flows Instabiity: Effects of Polymer versus Fibre Additives." *Jl of Non-Newtonian Fluid Mechanics*, Vol. 91, pp. 233-254.

BAKER, R. (2000). "The CIRIA Guide for the Design of Stepped-Block Spillways." *Intl Workshop on Hydraulics of Stepped Spillways*, Zürich, Switzerland, H.E. MINOR & W.H. HAGER Editors, Balkema Publ., pp. 155-161.

BANDYOPADHYAT, P.R. (1987). "Rough-Wall Turbulent Boundary Layers in the Transition Regime." *Jl of Fluid Mech.*, Vol. 180, pp. 231-266.

BEHNIA, M., and GILLESPIE, S.J. (1991). "Void Fraction Measurement by a Computerized Double-Point Resistivity Probe." *Flow Meas. Instrum.*, Vol. 2, oct., pp. 243-247.

BOES, R.M. (1999). "Physical Model Study on Two-Phase Cascade Flow." *Proc. 28th IAHR Congress*, Graz, Austria, Session S1, 6 pages (CD-ROM).

BOES, R.M. (2000). "Zweiphasenstroömung und Energieumsetzung auf Grosskaskaden." *Ph.D. thesis*, VAW-ETH, Zürich, Switzerland.

BOS, M.G. (1976). "Discharge Measurement Structures." *Publication No. 161*, Delft Hydraulic Laboratory, Delft, The Netherlands (also Publication No. 20, ILRI, Wageningen, The Netherlands).

CAIN, P. (1978). "Measurements within Self-Aerated Flow on a Large Spillway." *Ph.D. Thesis*, Ref. 78-18, Dept. of Civil Engrg., Univ. of Canterbury, Christchurch, New Zealand.

CHABOT, J., LEE, S.L.P., SORIA, A., and LASA, H.I. de (1992). "Interaction between Bubbles and Fibre Optic Probes in a Bubble Column." *Can. Jl of Chem. Eng.*, Vol. 70, Feb., pp. 61-68.

CHAMANI, M.R. (2000). "Air inception in Skimming Flow regime over Stepped Spillways." *Intl Workshop on Hydraulics of Stepped Spillways*, Zürich, Switzerland, H.E. MINOR & W.H.

HAGER Editors, Balkema Publ., pp. 61-67.

CHAMANI, M.R., and RAJARATNAM, N. (1999). "Characteristics of Skimming Flow over Stepped Spillways." *Jl of Hyd. Engrg.*, ASCE, Vol. 125, No. 4, pp. 361-368.

CHANSON, H. (1988). "A Study of Air Entrainment and Aeration Devices on a Spillway Model." *Ph.D. thesis*, Ref. 88-8, Dept. of Civil Engrg., University of Canterbury, New Zealand (ISSN 0110-3326).

CHANSON, H. (1993a). "Stepped Spillway Flows and Air Entrainment." *Can. Jl of Civil Eng.*, Vol. 20, No. 3, June, pp. 422-435.

CHANSON, H. (1993b). "Self-Aerated Flows on Chutes and Spillways." *Jl of Hyd. Engrg.*, ASCE, Vol. 119, No. 2, pp. 220-243. Discussion : Vol. 120, No. 6, pp. 778-782.

CHANSON, H. (1994) "Drag Reduction in Open Channel Flow by Aeration and Suspended Load." *Jl of Hyd. Res.*, IAHR, Vol. 32, No. 1, pp. 87-101.

CHANSON, H. (1995a). "Hydraulic Design of Stepped Cascades, Channels, Weirs and Spillways." *Pergamon*, Oxford, UK, Jan., 292 pages.

CHANSON, H. (1995b). "Air Bubble Diffusion in Supercritical Open Channel Flow." *Proc. 12th Australasian Fluid Mechanics Conference AFMC*, Sydney, Australia, R.W. BILGER Ed., Vol. 2, pp. 707-710.

CHANSON, H. (1995c). "Air Bubble Entrainment in Free-surface Turbulent Flows. Experimental Investigations." *Report CH46/95*, Dept. of Civil Engineering, University of Queensland, Australia, June, 368 pages.

CHANSON, H. (1996). "Prediction of the Transition Nappe/Skimming Flow on a Stepped Channel." *Jl of Hyd. Res.*, IAHR, Vol. 34, No. 3, pp. 421-429.

CHANSON, H. (1997a). "A Short History of Stepped Cascades in Australia." *ANCOLD Bulletin*, No. 106, Aug., pp. 101-111.

CHANSON, H. (1997b). "Air Bubble Entrainment in Free-Surface Turbulent Shear Flows." *Academic Press*, London, UK, 401 pages.

CHANSON, H. (1997c). "Measuring Air-Water Interface Area in Supercritical Open Channel Flow." *Water Res.*, IAWPRC, Vol. 31, No. 6, pp. 1414-1420.

CHANSON, H. (1999a). "Turbulent Open-Channel Flows : Drop-Generation and Self-Aeration.

Discussion." *Jl of Hyd. Engrg.*, ASCE, Vol. 125, No. 6, pp. 668-670.

CHANSON, H. (1999b). "The Hydraulics of Open Channel Flows : An Introduction." *Butterworth-Heinemann*, Oxford, UK, 512 pages. (Reprinted in 2001)

CHANSON, H. (2000). "Forum article. Hydraulics of Stepped Spillways: Current Status." *Jl of Hyd. Engrg.*, ASCE, Vol. 126, No. 9, pp. 636-637.

CHANSON, H. (2000b). "A Review of Accidents and Failures of Stepped Spillways and Weirs." *Proc. Instn Civ. Engrs Water and Maritime Engrg*, UK, Vol. 142, Dec., pp. 177-188.

CHANSON, H. (2001). "The Hydraulics of Stepped Chutes and Spillways." *Balkema Publ.*, Rotterdam, The Netherlands.

CHANSON, H., and BRATTBERG, T. (1998). "Air Entrainment by Two-Dimensional Plunging Jets : the Impingement Region and the Very-Near Flow Field." *Proc. 1998 ASME Fluids Eng. Conf.*, FEDSM'98, Washington DC, USA, June 21-25, Paper FEDSM98-4806, 8 pages (CD-ROM).

CHANSON, H., and TOOMBES, L. (1997). "Flow Aeration at Stepped Cascades." *Research Report No. CE155*, Dept. of Civil Engineering, University of Queensland, Australia, June, 110 pages.

CHANSON, H., and TOOMBES, L. (2000). "Stream Reaeration in Nonuniform Flow: Macroroughness Enhancement." *Jl of Hyd. Engrg.*, ASCE, Vol. 126, No. 3, pp. 222-224.

CHANSON, H., YASUDA, Y., and OHTSU, I. (2000). "Flow Resistance in Skimming Flow : a Critical Review." *Intl Workshop on Hydraulics of Stepped Spillways*, Zürich, Switzerland, H.E. MINOR & W.H. HAGER Editors, Balkema Publ., pp. 95-102.

CHANSON, H., and WHITMORE, R.L. (1998). "Gold Creek Dam and its Unusual Waste Waterway (1890-1997) : Design, Operation, Maintenance." *Can. Jl of Civil Eng.*, Vol. 25, No. 4, Aug., pp. 755-768 & Front Cover.

COOK, N.J. (1990). "The Designer's Guide to Wind Loading of Building Structures. Part 2 : Static Structures." *Building Research Establishment & Butterworths*, London, UK, 586 pages.

CROWE, C., SOMMERFIELD, M., and TSUJI, Y. (1998). "Multiphase Flows with Droplets and Particles." *CRC Press*, Boca Raton, USA, 471 pages.

DJENEDI, L, ANSELMET, F., and ANTONIA, R.A. (1994). "LDA Measurements in a Turbulent Boundary Layer over a D-Type Rough Wall." *Experiments in Fluids*, Vol. 16, pp. 323-329.

ELAVARASAN, R., PEARSON, B.R., and ANTONIA, R.E. (1995). "Visualization of Near Wall

Region in a Turbulent Boundary Layer over Transverse Square Cavities with Different Spacing." *Proc. 12th Australasian Fluid Mech. Conf. AFMC*, Sydney, Australia, Vol. 1, pp. 485-488.

ETHEMBABAOGLU (1978). "Some Characteristics of Unstable Flow Past Slots." *Jl of Hyd. Div.*, ASCE, Vol. 104, No. HY5, pp. 649-666.

FRIZELL, K.H. (1992). "Hydraulics of Stepped Spillways for RCC Dams and Dam Rehabilitations. " *Proc. 3rd Specialty Conf. on Roller Compacted Concrete*, ASCE, San Diego CA, USA, pp. 423-439.

HAUGEN, H.L., and DHANAK, A.M. (1966). "Momentum Transfer in Turbulent Separated Flow past a Rectangular Cavity." *Jl of Applied Mech.*, Trans. ASME, Sept., pp. 641-464.

HEIDRICK, T.R., BANERJEE, S., and AZAD, R.S. (1977). "Experiments on the Structure of Turbulence in Fully Developed Pipe Flow. Part 2. A Statistical Procedure for Identifying 'Bursts' in the Wall Layers and some Characteristics of Flow during Bursting Periods." *Jl of Fluid Mech.*, Vol. 82, Pt 4, pp. 705-723.

HORNER, M.W. (1969). "An Analysis of Flow on Cascades of Steps." *Ph.D. thesis*, Univ. of Birmingham, UK, May, 357 pages.

KELEN, N. (1933). "Gewichtsstaumauern und Massive Wehre." ('Gravity Dams and Large Weirs.') *Verlag von Julius Springer*, Berlin, Germany (in German).

KIPPHAN, H. (1977). "Bestimmung von Tranportkenngrößen bei Mehrphasenströmungen mit Hilfe *Chemie Ingenieur Technik*, Vol. 49, No. 9, pp. 695-707 (in German).

LAALI, A.R., and MICHEL, J.M. (1984). "Air Entrainment in Ventilated Cavities : Case of the Fully Developed 'Half- Cavity'." *Jl of Fluids Eng.*, Trans. ASME, Sept., Vol. 106, p.319.

LEWIS, D.A., and DAVIDSON, J.F. (1983). "Bubble Sizes Produced by Shear and Turbulence in a Bubble Column." *Chem. Eng. Sc.*, Vol. 38, No. 1, pp. 161-167.

LIU, T.J., and BANKOFF, S.G. (1993). "Structure of Air-water Bubbly Flow in a Vertical Pipe - II. Void Fraction, Bubble Velocity and Bubble Size Distribution." *Intl Jl of Heat and Mass Transfer*, Vol. 36, No. 4, pp. 1061-1072.

MATOS, J., SÁNCHEZ, M., QUINTELA, A., and DOLZ, J. (1999). "Characteristic Depth and Pressure Profiles in Skimming Flow over Stepped Spillways." *Proc. 28th IAHR Congress*, Graz, Austria, Session B14, 6 pages.

MATOS, J. (2000). "Hydraulic Design of Stepped Spillways over RCC Dams." *Intl Workshop on Hydraulics of Stepped Spillways*, Zürich, Switzerland, H.E. MINOR & W.H. HAGER Editors, Balkema Publ., pp. 187-194.

MICHEL, J.M. (1984). "Some Features of Water Flows with Ventilated Cavities." *Jl of Fluids Eng.*, Trans. ASME, Sept., Vol. 106, p.319.

MICHEL, J.M., and ROWE, A. (1974). "Profils Minces Supercavitants à Arrière Tronqué." *Jl La Houille Blanche*, Bo. 3, pp. 1-43.

NAUDASCHER, E. (1967). "From Flow Instability to Flow-Induced Excitation." *Jl of Hyd. Div.*, Proc. ASCE, Vol. 93, No. HY4, pp. 15-40.

NAUDASCHER, E., and ROCKWELL, D. (1994). "Flow-Induced Vibrations. An Engineering Guide." *IAHR Hydraulic Structures Design Manual No. 7*, Hydraulic Design Considerations, Balkema Publ., Rotterdam, The Netherlands, 413 pages.

OHTSU, I., and YASUDA, Y. (1997). "Characteristics of Flow Conditions on Stepped Channels." *Proc. 27th IAHR Biennal Congress*, San Francisco, USA, Theme D, pp. 583-588.

OHTSU, I, YASUDA, Y., and TAKAHASHI, M. (2000). "Characteristics of Skimming Flow over Stepped Spillways. Discussion." *Jl of Hyd. Engrg.*, ASCE, Vol. 126, No. 11, pp. 869-871.

OLIVIER, H. (1967). "Through and Overflow Rockfill Dams - New Design Techniques." *Proc. Instn. Civil Eng.*, March, 36, pp. 433-471. Discussion, 36, pp. 855-888.

RAJARATNAM, N. (1990). "Skimming Flow in Stepped Spillways." *Jl of Hyd. Engrg.*, ASCE, Vol. 116, No. 4, pp. 587-591. Discussion : Vol. 118, No. 1, pp. 111-114.

REVANKAR, S.T., and ISHII, M. (1992). "Local Interfacial Area Measurement in Bubbly Flow." *Intl Jl of Multiphase Flow*, Vol. 35, No. 4, pp. 913-925.

RIEDIGER, S. (1989). "Influence of Drag Reducing Additives on a Plane Mixing Layer." *Proc. 4th Intl Conf. on Drag Reduction*, Davos, Switzerland, Ellis Horwood Publ., Chichester, UK, No. 10.4, pp. 303-310.

ROUSE, H. (1937). "Modern Conceptions of the Mechanics of Turbulence." *Transactions*, ASCE, Vol. 102, pp. 463-543.

RUFF, J.F., and FRIZELL, K.H. (1994). "Air Concentration Measurements in Highly-Turbulent Flow on a Steeply-Sloping Chute." *Proc. Hydraulic Engineering Conf.*, ASCE, Buffalo, USA, Vol. 2,

pp. 999-1003.

SCHLICHTING, H. (1979). "Boundary Layer Theory." *McGraw-Hill*, New York, USA, 7th edition.

SCHUYLER, J.D. (1909). "Reservoirs for Irrigation, Water-Power and Domestic Water Supply." *John Wiley & sons*, 2nd edition, New York, USA.

SENE, K.J. (1984). "Aspects of Bubbly Two-Phase Flow." *Ph.D. thesis*, Trinity College, Cambridge, UK, Dec..

SERIZAWA, A., KATAOKA, I., and MICHIYOSHI, I. (1975). "Turbulence Structure of Air-Water Bubbly Flows - I. Measuring Techniques." *Intl Jl Multiphase Flow*, Vol. 2, No. 3, pp. 221-233

SHVAINSHTEIN, A.M. (1999). "Stepped Spillways and Energy Dissipation." *Gidrotekhnicheskoe Stroitel'stvo*, No. 5, pp. 15-21 (in Russian). (Also Hydrotechnical Construction, Vol. 3, No. 5, 1999, pp. 275-282.)

SILBERMAN, E., and SONG, C.S. (1961). "Instability of Ventilated Cavities." *Jl of Ship Res.*, Vol. 5, No. 1, pp. 13-33.

SPIEGEL, M.R. (1974). "Mathematical Handbook of Formulas and Tables." *McGraw-Hill Inc.*, New York, USA.

STRAUB, L.G., and ANDERSON, A.G. (1958). "Experiments on Self-Aerated Flow in Open Channels." *Jl of Hyd. Div.*, Proc. ASCE, Vol. 84, No. HY7, paper 1890, pp. 1890-1 to 1890-35.

SUMER, B.M., COKGOR, S., and FREDS∅E, J. (2001). "Suction Removal of Sediment from between Armor Blocks." *Jl of Hyd. Engrg.*, ASCE, Vo. 127, No. 4, pp. 293-306.

SURYANARAYANA, G.K., PAUER, H., and MEIER, G.E.A. (1993). "Bluff-Body Drag Reduction by Passive Ventilation." *Exp. in Fluids*, Vol. 16, pp. 73-81.

SURYANARAYANA, G.K., and PRABHU, A. (2000). "Effect of natural ventilation on the boundary layer separation and near-wake vortex shedding characteristics of a sphere." *Exp. in Fluids*, Vol. 19, No. 6, pp. 582-591.

TALBOT, J.R., ROBINSON, K.M., and KADAVY, P.E. (1997). "Hydrauic Model Study of a Roller Compacted Concrete Stepped Spillway with Converging Chute Walls." *Proc. Association of State Dam Safety Officials Annual Conf.*, Pittsburg PA, USA, 10 pages.

TANTIRIGE, S.C., IRIBARNE, A.P., OJHAS, M., and TRASS, O. (1994). "The Turbulent Boundary Layer over Single V-shaped Cavities." *Intl Jl Heat Mass Transfer*, Vol. 37, pp. 2261-2271.

TOOMBES, L., and CHANSON, H. (2000). "Air-Water Flow and Gas Transfer at Aeration Cascades: a Comparative Study of Smooth and Stepped Chutes." *Intl Workshop on Hydraulics of Stepped Spillways*, Zürich, Switzerland, H.E. MINOR & W.H. HAGER Editors, Balkema Publ., pp. 77-84.

TOWNES, H.W., and SABERSKY, R.H. (1966). "Experiments on the Flow over a Rough Surface." *Intl Jl of Heat and Mass Transfer*, Vol. 9, pp. 729-738.

TOZZI, M.J. (1992). "Caracterização/Comportamento de Escoamentos em Vertedouros com Paramento em Degraus." ('Hydraulics of Stepped Spillways.') *Ph.D. thesis*, University of Sao Paulo, Brazil (in Portuguese).

TOZZI, M., TANIGUCHI, E., and OTA, J. (1998). "Air Concentration in Flows over Stepped Spillways." *Proc. 1998 ASME Fluids Eng. Conf.*, FEDSM'98, Washington DC, USA, June 21-25, Paper FEDSM98-5053, 7 pages (CD-ROM).

TURNBULL, J.D., and McKAY, G.R. (1974). "The Design and Construction of Chinchilla Weir - Condamine River Queensland." *Proc. 5th Austalasian Conf. on Hydraulics and Fluid Mechanics*, Christchuch, New Zealand, Vol. II, pp. 1-8.

VERRON, J., and MICHEL, J.M. (1984). "Base-vented Hydrofoils of Finite Span under a Free Surface : an Experimental Investigation." *Jl of Ship Res.*, Vol. 28, No. 2, pp. 90-106.

WEGMANN, E. (1907). "The Design of the New Croton Dam." *Transactions*, ASCE, Vol. LXVIII, No. 1047, pp. 398-457.

WEGMANN, E. (1911). "The Design and Construction of Dams." *John Wiley & Sons*, New York, USA, 6th edition.

WOOD, C.J. (1964). "The Effect of Base Bleed on periodic Wake." *Jl Roy. Aeronautical Soc.*, Vol. 68, pp. 477-482.

WOOD, I.R. (1983). "Uniform Region of Self-Aerated Flow." *Jl Hyd. Eng.*, ASCE, Vol. 109, No. 3, pp. 447-461.

WOOD, I.R. (1985). "Air Water Flows." *Proc. 21st IAHR Congress*, Melbourne, Australia, Keynote address, pp. 18-29.

WOOD, I.R. (1991). "Air Entrainment in Free-Surface Flows." *IAHR Hydraulic Structures Design Manual No. 4*, Hydraulic Design Considerations, Balkema Publ., Rotterdam, The Netherlands, 149 pages.

XI, Ruze (1988). "Characteristics of Self-Aerated Flow on Steep Chutes." *Proc. Intl Symp. on Hydraulics for High Dams*, IAHR, Beijing, China, pp. 68-75.

YASUDA, Y., and OHTSU, I. (1999). "Flow Resistance of Skimming Flow in Stepped Channels." *Proc. 28th IAHR Congress*, Graz, Austria, Session B14, 6 pages (CD-ROM).

YASUDA, Y., and OHTSU, I. (2000). "Characteristics of Plunging Flows in Stepped Channel Chutes." *Intl Workshop on Hydraulics of Stepped Spillways*, Zürich, Switzerland, H.E. MINOR & W.H. HAGER Editors, Balkema Publ., pp. 147-152.

Internet Resources

Overflow embankment stepped spillways. Earth dam spillways with precast concrete blocks	http://www.uq.edu.au/~e2hchans/over_st.html
The Minimum Energy Loss (MEL) weir design. An overflow earthfill embankment dam	http://www.uq.edu.au/~e2hchans/mel_weir.html
Self-aeration on chute and stepped spillways - Air entrainment and flow aeration in open channel flows	http://www.uq.edu.au/~e2hchans/self_aer.html
Timber Crib Weirs in Queensland, Australia	http://www.uq.edu.au/~e2hchans/tim_weir.html
Current expertise and experience on stepped channel flows	http://www.uq.edu.au/~e2hchans/dpri/topic_2.html

The bibliographic reference of the present report is :

CHANSON, H., and TOOMBES, L. (2001). "Experimental Investigations of Air Entrainment in Transition and Skimming Flows down a Stepped Chute. Application to Embankment Overflow Stepped Spillways." *Research Report No. CE158*, Dept. of Civil Engineering, The University of Queensland, Brisbane, Australia, July (ISBN 1 864995297).

The Research Report CE158 is available, in the present form, as a .PDF file on the Internet at the following address :

http://www.uq.edu.au/~e2hchans/reprints/ce158.pdf